

Fracton Topological Order from Nearest-Neighbor Two-Spin Interactions and Dualities

Kevin Slagle¹ and Yong Baek Kim^{1,2}

¹*Department of Physics, University of Toronto,
Toronto, Ontario M5S 1A7, Canada*

²*Canadian Institute for Advanced Research,
Toronto, Ontario, M5G 1Z8, Canada*

Fracton topological order describes a remarkable phase of matter which can be characterized by fracton excitations with constrained dynamics and a ground state degeneracy that increases exponentially with the length of the system on a three-dimensional torus. However, previous models exhibiting this order require many-spin interactions which may be very difficult to realize in a real material or cold atom system. In this work, we present a more physically realistic model which has the so-called X-cube fracton topological order [1] but only requires nearest-neighbor two-spin interactions. The model lives on a three-dimensional honeycomb-based lattice with one to two spin-1/2 degrees of freedom on each site and a unit cell of 6 sites. The model is constructed from two orthogonal stacks of Z_2 topologically ordered Kitaev honeycomb layers [2], which are coupled together by a two-spin interaction. It is also shown that a four-spin interaction can be included to instead stabilize 3+1D Z_2 topological order. We also find dual descriptions of four quantum phase transitions in our model, all of which appear to be discontinuous first order transitions.

I. INTRODUCTION

Quantum phases with fracton topological order [3–9] have recently received much attention. [10–13] These phases can be characterized as having topological excitations, called fractons [9], which are immobile (when isolated from other fractons [14]), and for having large degeneracies (on a torus) which can be sub-extensive: e.g. $\text{degen} \sim 2^L$ for a 3D torus of length L . Fracton order has applications including self-correcting quantum memory for quantum computers [7, 15, 16], and even emergent gravity given a finite density of (possibly gapless) fractons [14].

However, most models of fracton order require many-spin interactions, which seems difficult to realize in a real material or cold atom system. For example, the so-called X-cube order requires a 12-spin interaction term [1]. Recently, it has been shown [17, 18] that X-cube order can be constructed by coupling together three orthogonal stacks of intersecting two-dimensional toric codes [19], requiring only 4-spin interactions. Unfortunately, 4-spin interactions can also be difficult to realize in a physical system. On the other hand, in Ref. [2] Kitaev presents a honeycomb lattice model with only 2-spin interactions which, in a certain large coupling limit, has an effective Hamiltonian described by toric code. In Sec. II, we combine these ideas to produce a more realistic model of fracton order which only requires nearest-neighbor 2-spin interactions. Our model consists of two orthogonal stacks of Kitaev honeycomb models, which intersect on certain shared links. To induce fracton order, we add a large two-spin coupling on the shared links to couple together the orthogonal layers.

Ref. [17] also showed that their isotropic coupled layer construction admits a duality describing a first order

phase transition out of X-cube fracton topological order. Additionally, Ref. [1] gave dualities describing phase transitions out of an entire class of fracton phases; however, the nature of these phase transitions is currently unknown. In this work, we find two new dualities which describe two different quantum phase transitions out of the X-cube phase which both appear to be discontinuous first order transitions. The dual descriptions of the two phase transitions are described by a grid of weakly coupled 1+1D transverse-field Ising models, or a stack of decoupled 2+1D transverse-field Ising models. These dualities are summarized in Fig. 1 and are described in detail in Sec. III.

Although a single layer of a 1+1D or 2+1D transverse-field Ising model hosts a continuous quantum phase transition, this isn't necessarily the case when they are weakly coupled together. The dual theories in our model allow the 1+1D or 2+1D Ising layers to be coupled together as long as a subdimensional Ising symmetry which flips all spins on any given layer is preserved. Therefore, a $\phi_L^2 \phi_{L'}^2$ term (in a stack of ϕ^4 field theories) or $\sigma_{L'I}^z \sigma_{L'J}^z \sigma_{L'I}^z \sigma_{L'J}^z$ term (in a stack of transverse-field Ising models) is symmetry allowed, where L and L' denote neighboring layers, and I and J are nearest-neighbor sites on a layer. ($\phi_L \phi_{L'}$ or $\sigma_{L'I}^z \sigma_{L'J}^z$ are odd under subdimensional symmetry and thus not allowed.) In Appendix C we give classical Monte Carlo evidence that these symmetry allowed perturbations are relevant under RG (renormalization group) and that the transitions are likely to be discontinuous first order transitions. That is, for small but finite layer coupling, we find evidence of first order transitions; but we can not rule out the possibility that smaller layer couplings could result in a continuous phase transition. We also find intermediate phases with topological (possibly with fractons) order

and spontaneous translation symmetry breaking when the sign of the layer coupling is negative.

In Sec. IV we also consider an extended model where we introduce a different interaction term to couple together the intersecting honeycomb layers (and an infinitesimal perturbation to break accidental symmetry). Similar to the previous coupled layer constructions [17, 18], when this coupling is large, 3+1D Z_2 topological order is stabilized. However, when both this coupling and the coupling that resulted in X-cube order are large, a stack of 2+1D Z_2 topological order is stabilized on planes orthogonal to the original two stacks of honeycomb lattices. This result differs from the previous coupled layer constructions [17, 18] which obtain a trivial state when both couplings are large. This difference occurs because our construction is built from only two orthogonal stacks of 2+1D Z_2 topological order, while the previous constructions used three stacks. In Sec. IV C we give a global duality description for four (most likely first order) phase transitions in the extended model by mapping to decoupled 2+1D and 1+1D transverse-field Ising models, which is summarized in Fig. 1. In Sec. IV D we discuss connections to previous coupled layer constructions [17, 18]. Finally, in Sec. V we conclude with possible future directions.

II. NEAREST-NEIGHBOR FRACTON MODEL

The model lives on a 3 dimensional lattice, shown in Fig. 2, of two orthogonal stacks of honeycomb lattices: one stack consisting of a honeycomb lattice on an XY plane for each $z \in \mathbb{Z}$, and the other stack on XZ planes for each $y \in \mathbb{Z}$. Some of the links (dark-blue in Fig. 2) of each honeycomb lattice will overlap with a link on an orthogonal honeycomb lattice. We will refer to these links as ‘‘shared links’’, and the sites on each end of a shared link will be referred to as ‘‘shared sites’’. There will be a spin-1/2 degree of freedom on every site of the honeycomb lattices, which means that there will be two spin-1/2 on each shared site. The spins on the XY and XZ planes will be labeled σ^μ and τ^μ , respectively.

The Hamiltonian is given by

$$H = H_K + H_t \quad (1)$$

$$H_K = - \sum_{\mu=x,y,z} \sum_{\langle ij \rangle}^{\mu\text{-links}} \begin{cases} K_\mu \sigma_i^\mu \sigma_j^\mu & \sigma\text{-link} \\ K_\mu \tau_i^\mu \tau_j^\mu & \tau\text{-link} \\ K_z (\sigma_i^z \sigma_j^z + \tau_i^z \tau_j^z) & \text{shared-link} \end{cases} \quad (2)$$

$$H_t = - \sum_{\langle ij \rangle}^{\text{shared-links}} \frac{t}{2} (\sigma_i^z \tau_i^z + \sigma_j^z \tau_j^z) \quad (3)$$

In Sec. IV, we will discuss an alternate coupling that can produce 3+1D Z_2 topological order. A rough phase

diagram for this model is given in Fig. 3. The signs of all coefficients in H (i.e. K_μ and t , and also h and h' in H' , which is defined later in Eq. (25)) will be taken to be positive.

H_K is a sum of Kitaev honeycomb models [2] on each honeycomb lattice. $\sum_{\mu=x,y,z}$ sums over the different kinds of links (x =red, y =green, z =blue in Fig. 2), and $\sum_{\langle ij \rangle}^{\mu\text{-links}}$ sums over all links of type μ . A link is also referred to as a σ -link (or τ -link) if it is a link on either a XY (or XZ) honeycomb plane. If a link is shared by both an XY and XZ honeycomb plane, then it is instead referred to as a shared-link. K_x, K_y, K_z are couplings across the different bond types. If we only consider H_K , then the ground state will have decoupled 2+1D Z_2 topological order on each honeycomb lattice, and will be gapped when $K_z > K_x + K_y$ [2].

H_t couples the 2D honeycomb lattices together. H_t consists of a $\sigma_i^z \tau_i^z$ coupling on every shared site. In Sec. II B we argue that this term will cause loops of fluxes to condense, which will result in X-cube fracton topological order when K_z and t are large.

A. Decoupled Phase: XY&XZ plane 2+1D Z_2 Topological Order

Before explaining the fracton phase, we will first review the $t = 0$ case with $\max(K_x, K_y) \ll K_z$. In this limit, the XY and XZ-plane hexagon lattices are completely decoupled from each other, and each form a Kitaev honeycomb model [2]. In Fig. 4, we show a honeycomb lattice on the XY plane. When $\max(K_x, K_y) \ll K_z$, degenerate perturbation theory results in the following effective Hamiltonian (ignoring subleading terms) [2]:

$$\begin{aligned} H_{\text{toric}} &= H_{\text{toric}}^{\text{XY}} + H_{\text{toric}}^{\text{XZ}} \quad (4) \\ H_{\text{toric}}^{\text{XY}} &= - \sum_{p=\square}^{\text{XY planes}} E_\square [\sigma]_p^{\square\text{xy}} - \sum_{\iota=+}^{\text{XY plane}} E_+ [\sigma]_\iota^{+\text{xy}} \\ H_{\text{toric}}^{\text{XZ}} &= - \sum_{p=\square}^{\text{XZ planes}} E_\square [\tau]_p^{\square\text{xz}} - \sum_{\iota=+}^{\text{XZ plane}} E_+ [\tau]_\iota^{+\text{xz}} \\ E_\square &\sim E_+ \sim \frac{K_x^2 K_y^2}{K_z^3} \quad (\text{when } t = 0) \end{aligned}$$

$[\sigma]_p^{\square\text{xy}}, [\tau]_p^{\square\text{xz}}, [\sigma]_\iota^{+\text{xy}}, [\tau]_\iota^{+\text{xz}}$ are defined in Fig. 4

$\sum_{p=\square}^{\text{XY planes}}$ sums over plaquettes p that lie on an XY plane and $\sum_{\iota=+}^{\text{XY plane}}$ sums over vertices ι that lie on an XY plane (see Fig. 4). $\sum_{p=\square}^{\text{XZ planes}}$ and $\sum_{\iota=+}^{\text{XZ plane}}$ are similar, but instead sum over XZ planes. $[\sigma]_p^{\square\text{xy}}$ and $[\sigma]_\iota^{+\text{xy}}$ are defined in Fig. 4 and are closely related to the plaquette/flux and vertex/charge operators in Kitaev’s toric code [19]. $[\sigma]_p^{\square\text{xy}}$ and $[\sigma]_\iota^{+\text{xy}}$ are centered on

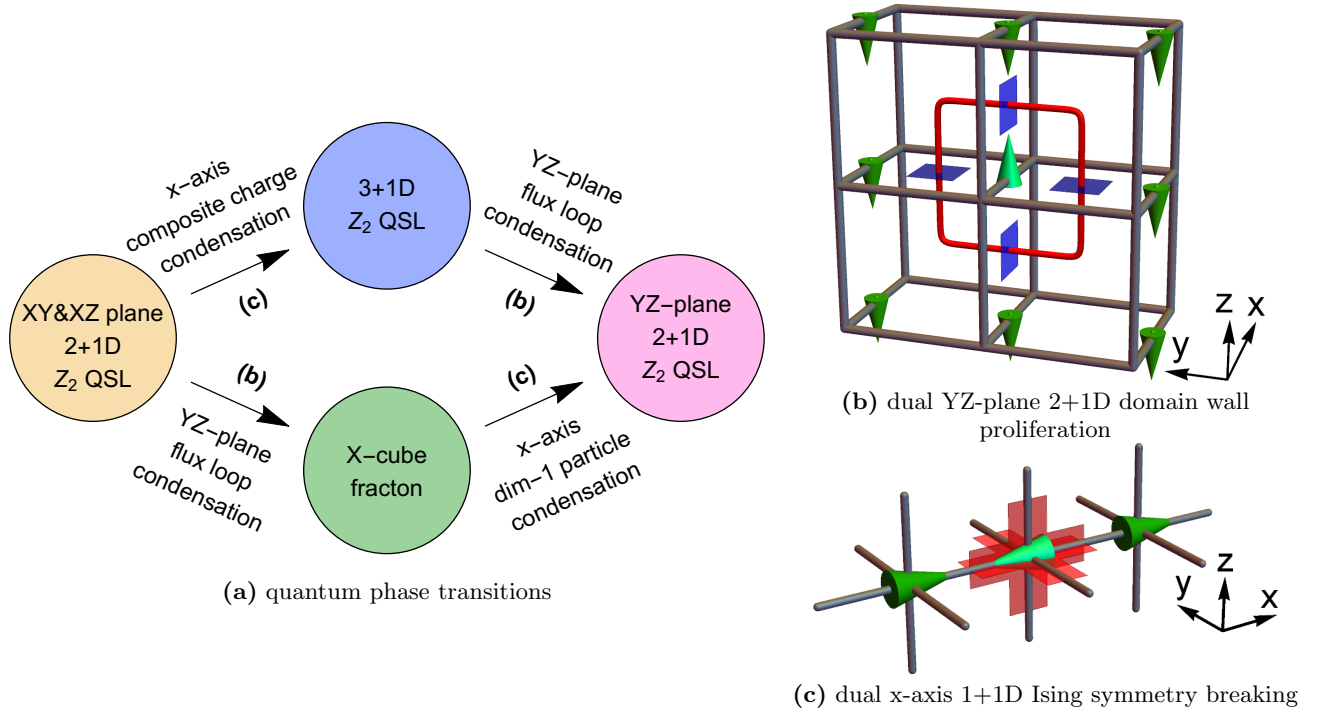


FIG. 1. Two series of condensation driven phase transitions with dual descriptions ((b) and (c)), which are described in Sec. III and Sec. IV C. All four phase transitions appear to be first order when generic perturbations are added (Appendix C). The transition from XY & XZ plane 2+1D Z_2 quantum spin liquid (QSL) to X-cube fracton topological order is driven by a condensation of YZ-plane composite flux loops (red loop in (b)), which are excitations of a loop of XY and XZ-plane 2+1D toric code flux operators ($[\tilde{\sigma}]_p^{\square XY}$ and $[\tilde{\tau}]_p^{\square XZ}$ in Sec. III A). In the dual theory, the YZ-plane flux loop is mapped to a YZ-plane domain wall excitation of Ising spins (green cones in (b), η_i^z in Sec. III A). The transition from X-cube fracton to a YZ-plane 2+1D Z_2 QSL is driven by a condensation of dimension-1 X-cube particle excitations (red cross in (c), $[\hat{\rho}]_i^{+XY}$ and $[\hat{\rho}]_i^{+XZ}$ in Sec. III B) which are bound to 1D lines parallel to the x-axis. In the dual theory, these x-axis particle excitations are mapped to excitations (light green cone $|\leftarrow\rangle$) in (c), μ_i^x in Sec. III B) of 1+1D Ising paramagnets, which spontaneously break a Z_2 Ising symmetry when they condense since they are conserved modulo two. The transition from XY & XZ plane QSL to 3+1D QSL is driven by condensing a composite of XY and XZ-plane 2+1D toric code charge excitations (red cross in (c)), which is also dual to a 1+1D Ising paramagnet excitation. The transition from 3+1D QSL to YZ-plane QSL is driven by condensing YZ-plane flux loops (red in (b)) in 3+1D toric code, which are dual to 2+1D Ising domain walls. These dualities also describe phase transitions shown in Fig. 3 and Fig. 8.

the plaquettes p and vertices ι , respectively, of the XY plane rectangular lattice (gray in Fig. 4). τ operators are similar, but instead live on XZ planes. In Fig. 5, we show the 3 dimensional lattice again, but with the intersecting rectangular toric code lattices also drawn. A more detailed calculation is done in Appendix A 1, with excitation energies E_{\square} and E_+ given for nonzero t (Eq. (A1)).

across every z -link:

$$\begin{aligned} \sigma_i^z \sigma_j^z &\rightarrow \begin{cases} 1 & \sigma\text{-link} \\ 1 & \text{shared-link} \end{cases} \\ \sigma_i^z \sigma_j^0 \ \&\ \sigma_i^0 \sigma_j^z &\rightarrow \begin{cases} \tilde{\sigma}_\ell^z & \sigma\text{-link} \\ \tilde{\sigma}_\ell^x & \text{shared-link} \end{cases} \\ \sigma_i^x \sigma_j^y &\rightarrow \begin{cases} \tilde{\sigma}_\ell^x & \sigma\text{-link} \\ \tilde{\sigma}_\ell^z & \text{shared-link} \end{cases} \end{aligned} \quad (5)$$

It is useful to do a change of basis and projection into the low energy Hilbert space where the energy of the large K_z term in H (Eq. (1)) is minimized with $\sigma_i^z \sigma_j^z = 1$

$$\begin{aligned} \tau &\rightarrow \tilde{\tau} \text{ is obtained by } \sigma \leftrightarrow \tau \\ H_{\text{toric}} &\rightarrow \tilde{H}_{\text{toric}} = \tilde{H}_{\text{toric}}^{\text{XY}} + \tilde{H}_{\text{toric}}^{\text{XZ}} \end{aligned} \quad (6)$$

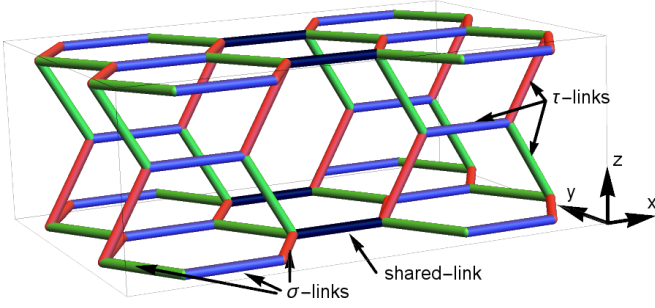


FIG. 2. The lattice that we consider: orthogonal stacks of honeycomb lattices along the XY and XZ planes which intersect on the dark-blue links, which we refer to as shared links in the text. σ^μ and τ^μ spin-1/2 degrees of freedom reside on sites of the XY and XZ honeycomb lattices, respectively. Thus, the shared sites on either end of a dark-blue link host both a σ^μ and τ^μ spin. The unit cell consists of 8 spins: the spins on both sides of a σ -link, a τ -link, and a shared-link which has two spins on each side. On each honeycomb lattice we impose a Kitaev honeycomb model (Eq. (2)) where the links are colored red (x -link), green (y -link), or (dark) blue (z -link) to indicate the kind of coupling in Eq. (2): $\sigma_i^x \sigma_j^x$, $\sigma_i^y \sigma_j^y$, $\sigma_i^z \sigma_j^z$ respectively (and similar for τ^μ). To induce X-cube fracton topological order, we place a strong $\sigma_i^z \tau_i^z$ coupling on every shared site.

$$\begin{aligned} \tilde{H}_{\text{toric}}^{\text{XY}} &= - \sum_{p=\square}^{\text{XY planes}} E_{\square} [\tilde{\sigma}]_p^{\square \text{xy}} - \sum_{\iota=+}^{\text{XY plane}} E_{+} [\tilde{\sigma}]_{\iota}^{+\text{xy}} \\ \tilde{H}_{\text{toric}}^{\text{XZ}} &= - \sum_{p=\square}^{\text{XZ planes}} E_{\square} [\tilde{\tau}]_p^{\square \text{xz}} - \sum_{\iota=+}^{\text{XZ plane}} E_{+} [\tilde{\tau}]_{\iota}^{+\text{xz}} \end{aligned}$$

$$\begin{aligned} [\sigma]_p^{\square \text{xy}} &\rightarrow [\tilde{\sigma}]_p^{\square \text{xy}} = \prod_{\ell \in \square} \tilde{\sigma}_{\ell}^z, & [\sigma]_{\iota}^{+\text{xy}} &\rightarrow [\tilde{\sigma}]_{\iota}^{+\text{xy}} = \prod_{\ell \in +} \tilde{\sigma}_{\ell}^x \\ [\tau]_p^{\square \text{xz}} &\rightarrow [\tilde{\tau}]_p^{\square \text{xz}} = \prod_{\ell \in \square} \tilde{\tau}_{\ell}^z, & [\tau]_{\iota}^{+\text{xz}} &\rightarrow [\tilde{\tau}]_{\iota}^{+\text{xz}} = \prod_{\ell \in +} \tilde{\tau}_{\ell}^x \end{aligned}$$

Thus, we are projecting into the $\sigma_i^z \sigma_j^z = 1$ subspace and doing a unitary rotation on the shared-links. σ_i^0 (e.g in $\sigma_i^0 \sigma_j^z \rightarrow \tilde{\sigma}_{\ell}^z$) is an identity operator, and is only written to emphasize that i and j are the sites on the two sides of the link ℓ . We will use a tilde to denote operators in this new basis. In this basis, the operators $[\sigma]_p^{\square \text{xy}} \rightarrow [\tilde{\sigma}]_p^{\square \text{xy}}$ and $[\sigma]_{\iota}^{+\text{xy}} \rightarrow [\tilde{\sigma}]_{\iota}^{+\text{xy}}$ (also given in Fig. 4) in \tilde{H}_{toric} exactly reproduce the flux and charge operators in Kitaev's toric code [19]. Therefore, when $t = 0$ and $\max(K_x, K_y) \ll K_z$, our model (Eq. (3)) is in a decoupled phase where every honeycomb lattice on an XY or XZ plane hosts its own gapped 2+1D Z_2 topological order. This is the ‘‘XY&XZ plane 2+1D Z_2 QSL’’ phase in Fig. 3.

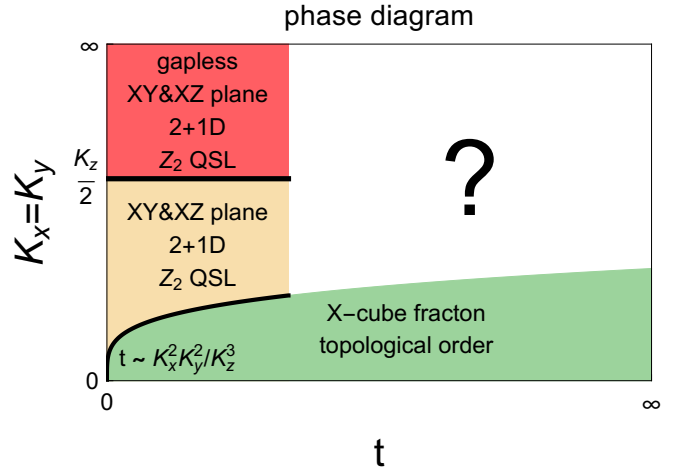


FIG. 3. Rough phase diagram of the Hamiltonian in Eq. (1) as a function of t (horizontal axis) and $K_x = K_y$ (vertical axis); K_z will be used to set the energy scale. When $t = 0$, the model consists of two orthogonal stacks (along the XY and XZ planes) of decoupled honeycomb lattices (Fig. 2), where each honeycomb lattice will host a quantum spin liquid (QSL) with Z_2 topological order, which will be gapped when $K_x = K_y < K_z/2$ and gapless when $K_x = K_y \geq K_z/2$ [2]. These QSL phases are stable to a small coupling t which couples the orthogonal honeycomb lattices together. (The gapless QSL is stable since t preserves time reversal symmetry; see e.g. Sec. 6.1 of Ref. [2].) In Sec. II B and Appendix A 2 we argue that X-cube fracton topological order [1] results when $\max(K_x, K_y) \ll \min(K_z, t)$. We do not know what phase(s) occur in the white region. In the bottom left corner, a phase transition between the QSL and fracton orders occurs near $t \sim K_x^2 K_y^2 / K_z^3$ (in the $\max(K_x, K_y) \ll K_z$ limit), which can be inferred from Fig. 11 in the appendix. In Sec. III A we propose that this transition is dual to a stack 2+1D Ising transitions; in Appendix C we find that the transition is likely first order and that (depending on the sign of certain perturbations) a topologically ordered intermediate phase is also possible.

B. X-Cube Fracton Phase

In this section, we will explain how X-cube fracton topological order results from our model H (Eq. (1)) in the limit

$$\max(K_x, K_y) \ll t \ll K_z \quad (7)$$

More generally, in the Appendix A 2 we show that $\max(K_x, K_y) \ll \min(t, K_z)$ is a sufficient condition for X-cube order. However, Eq. (7) allows us to apply the results from the previous section and is more closely connected to the previous layer constructions in Ref. [17, 18], and so we will discuss this limit in the main text and consider the more general condition (Eq. (A3)) in the appendix.

Thus, we will start from the decoupled $t = 0$ limit discussed in the previous section, and then make t very

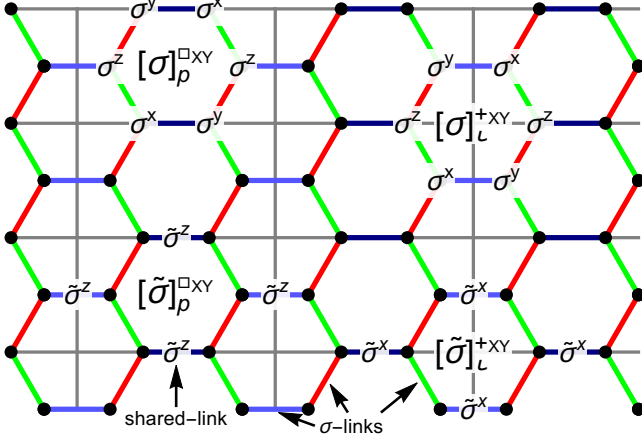


FIG. 4. An XY plane honeycomb lattice: a constant z slice of Fig. 2. There is a σ^μ degree of freedom on every site, and also a τ^μ on every shared-site: i.e. every site next to a dark-blue shared-link, which overlap gray lines. Red, green, and blue links host a $K_x\sigma_i^x\sigma_j^x$, $K_y\sigma_i^y\sigma_j^y$, or $K_z\sigma_i^z\sigma_j^z$ coupling, respectively. When $\max(K_x, K_y) \ll K_z$, degenerate perturbation theory will produce the operators $[\sigma]_p^{\square XY}$ (top-left) and $[\sigma]_\ell^{+XY}$ (top-right), which both take the form $\sigma_{i_1}^z\sigma_{i_2}^y\sigma_{i_3}^x\sigma_{i_4}^z\sigma_{i_5}^y\sigma_{i_6}^x$ for sites around a hexagon, as shown above. The low energy Hilbert space will have $\sigma_i^z\sigma_j^z = 1$ across all blue links; and so we will perform a local change of basis (and projection) $\sigma \rightarrow \tilde{\sigma}$ given in Eq. (5) to describe the effective low energy Hilbert space; the new $\tilde{\sigma}^\mu$ operators are centered on the blue links. In the $\tilde{\sigma}$ basis, $[\sigma]_p^{\square XY} \rightarrow [\tilde{\sigma}]_p^{\square XY}$ (bottom-left) and $[\sigma]_\ell^{+XY} \rightarrow [\tilde{\sigma}]_\ell^{+XY}$ (bottom-right) take the form of toric code flux and charge operators, as shown above. The gray lines indicate the rectangular lattice of the toric code. The XZ planes are similar, but with the replacement $\sigma \leftrightarrow \tau$. See Fig. 5 for a 3 dimensional version.

large. In the toric code basis (Eq. (5)), H (Eq. (1)) becomes:

$$H \rightarrow \tilde{H} = \tilde{H}_{\text{toric}} + \tilde{H}_t \quad (8)$$

$$H_t \rightarrow \tilde{H}_t = - \sum_{\ell}^{\text{shared-links}} t \tilde{\sigma}_\ell^x \tilde{\tau}_\ell^x \quad (9)$$

where \tilde{H}_{toric} was given in Eq. (6). We see that \tilde{H}_t couples the XY and XZ-planes together on the shared-links (gray links parallel to x-axis in Fig. 5) with a $\tilde{\sigma}_\ell^x \tilde{\tau}_\ell^x$ coupling. When acting on the decoupled $t = 0$ ground state, $\tilde{\sigma}_\ell^x \tilde{\tau}_\ell^x$ creates two $[\tilde{\sigma}]_p^{\square XY}$ and two $[\tilde{\tau}]_p^{\square XZ}$ excitations on the four plaquettes (of the gray cubic lattice in Fig. 5) that neighbor the link ℓ . When t is large, these excitations condense and the result is X-cube fracton topological order. (A similar condensation process is described in Ref. [17] and [18]; see Sec. IVD for connections.)

We will derive this result using degenerate perturba-

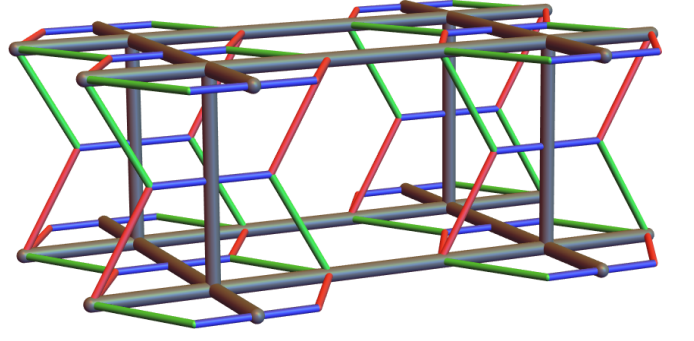


FIG. 5. The lattice that we consider (Fig. 2), except we also draw gray lines (as in Fig. 4) to indicate the intersecting rectangular lattices of the toric code (Eq. (4)) on XY and XZ planes.

tion theory (DPT). First, we split H (Eq. (1)) into

$$\begin{aligned} H &= H_0 + H_1 \\ H_0 &= \tilde{H}_t \\ H_1 &= \tilde{H}_{\text{toric}} \end{aligned} \quad (10)$$

where H_0 is the unperturbed Hamiltonian, H_1 is the perturbing Hamiltonian, and \tilde{H}_{toric} (Eq. (6)) was derived in the previous section. Eq. (7) is sufficient to ensure that DPT converges.

The effective Hamiltonian of the low energy Hilbert space is given by (see Appendix B for details):

$$\begin{aligned} H^{\text{eff}} &= \sum_{n=1}^{\infty} \mathcal{P}(H_1 \mathcal{D})^{n-1} H_1 \mathcal{P} + \dots \quad (11) \\ \mathcal{P} &= \prod_{\ell}^{\text{shared-links}} \frac{1}{2} (1 + \tilde{\sigma}_\ell^x \tilde{\tau}_\ell^x) \\ \mathcal{D} &= - \frac{1 - \mathcal{P}}{H_0 - E_0} \end{aligned}$$

\mathcal{P} projects into the low energy Hilbert space where $H_0 = \tilde{H}_t$ is minimized. \mathcal{D} projects onto states not in the low energy Hilbert space and penalizes energy excitations by a factor $1/(H_0 - E_0)$ where E_0 is the (degenerate) ground state energy of H_0 . “...” contains many terms (e.g. $-\frac{1}{2}\mathcal{P}H_1\mathcal{D}^2H_1\mathcal{P}H_1\mathcal{P}$); but these more complicated terms will be subleading corrections in this section. $[\tilde{\sigma}]_\ell^{+XY}$ and $[\tilde{\tau}]_\ell^{+XZ}$ (in $H_1 = \tilde{H}_{\text{toric}}$) commute with H_t (Eq. (3)), which implies that they do not create excitations out of the low energy Hilbert space. However, $[\tilde{\sigma}]_p^{\square XY}$ and $[\tilde{\tau}]_p^{\square XZ}$ do not commute with \tilde{H}_t , since \tilde{H}_t creates two $[\tilde{\sigma}]_p^{\square XY}$ and two $[\tilde{\tau}]_p^{\square XZ}$ excitations. Viewed differently, $[\tilde{\sigma}]_p^{\square XY}$ and $[\tilde{\tau}]_p^{\square XZ}$ create \tilde{H}_t excitations, which are not in the low energy Hilbert space. Therefore, $[\tilde{\sigma}]_\ell^{+XY}$ and $[\tilde{\tau}]_\ell^{+XZ}$ will be contained in H^{eff} but $[\tilde{\sigma}]_p^{\square XY}$ and $[\tilde{\tau}]_p^{\square XZ}$ will not.

We must now consider higher order terms ($n \geq 2$) in H^{eff} (Eq. (11)) to discover what role $[\tilde{\sigma}]_p^{\square XY}$ and $[\tilde{\tau}]_p^{\square XZ}$

end up playing. The first nonzero term involving $[\tilde{\sigma}]_p^{\square xy}$ or $[\tilde{\tau}]_p^{\square xz}$ is $E_{\text{cube}}[\tilde{\sigma}, \tilde{\tau}]_c^{\text{cube}}$, which is obtained at fourth order ($n = 4$), and the resulting effective Hamiltonian is

$$H^{\text{eff}} = \tilde{H}_{\text{X-cube}} + \dots$$

$$\begin{aligned} \tilde{H}_{\text{X-cube}} = & - \sum_{\iota=+}^{\text{XY planes}} E_+ [\tilde{\sigma}]_{\iota}^{+\text{xy}} - \sum_{\iota=+}^{\text{XZ planes}} E_+ [\tilde{\tau}]_{\iota}^{+\text{xz}} \\ & - \sum_{c=\text{cube}} E_{\text{cube}} [\tilde{\sigma}, \tilde{\tau}]_c^{\text{cube}} \end{aligned} \quad (12)$$

$$E_{\text{cube}} \sim \frac{E_{\square}^4}{t^3} \sim \frac{K_x^8 K_y^8}{K_z^{12} t^3} \quad \text{assuming (7)} \quad (13)$$

$[\tilde{\sigma}, \tilde{\tau}]_c^{\text{cube}}$ is defined in Fig. 6

$\sum_{c=\text{cube}}$ sums over the cubes c shown in Fig. 5. $[\tilde{\sigma}, \tilde{\tau}]_c^{\text{cube}}$ is the product of two XY-plane plaquette $[\tilde{\sigma}]_p^{\square xy}$ and two XZ-plane plaquette $[\tilde{\tau}]_p^{\square xz}$ operators around a cube (Fig. 6). Note that $[\tilde{\sigma}, \tilde{\tau}]_c^{\text{cube}}$ commutes with \tilde{H}_t , and can therefore appear in the effective Hamiltonian since it preserves the low energy Hilbert space. The “...” in H^{eff} denotes other subleading terms generated by DPT which are not important. Another round of DPT on H^{eff} with an unperturbed Hamiltonian $H'_0 = \tilde{H}_{\text{X-cube}}$ (and perturbation $H'_1 = H^{\text{eff}} - \tilde{H}_{\text{X-cube}}$) will eliminate terms in “...” which anticommute with $\tilde{H}_{\text{X-cube}}$, resulting in an exactly solvable effective Hamiltonian with the same ground state as $\tilde{H}_{\text{X-cube}}$. The “~” in the energy expressions means that these expressions are only asymptotically correct (in the $\max(K_x, K_y) \ll t \ll K_z$ limit); e.g. factors of two are ignored.

It is again useful to do a change of basis and projection into the low energy Hilbert space where now the energy of H_0 is minimized with $\tilde{\sigma}_{\ell}^x \tilde{\tau}_{\ell}^x = 1$ on every shared-link:

$$\begin{aligned} \sigma\text{-links:} & \quad \tilde{\sigma}_{\ell}^{\mu} \rightarrow \hat{\rho}_{\ell}^{\mu} \\ \tau\text{-links:} & \quad \tilde{\tau}_{\ell}^{\mu} \rightarrow \hat{\rho}_{\ell}^{\mu} \\ \text{shared-links:} & \quad \tilde{\sigma}_{\ell}^x \tilde{\tau}_{\ell}^x \rightarrow 1 \\ & \quad \tilde{\sigma}_{\ell}^x \rightarrow \hat{\rho}_{\ell}^x \\ & \quad \tilde{\sigma}_{\ell}^z \tilde{\tau}_{\ell}^z \rightarrow \hat{\rho}_{\ell}^z \end{aligned} \quad (14)$$

$$\tilde{H}_{\text{X-cube}} \rightarrow \hat{H}_{\text{X-cube}} = \quad (15)$$

$$- \sum_{\iota=+}^{\text{XY planes}} E_+ [\hat{\rho}]_{\iota}^{+\text{xy}} - \sum_{\iota=+}^{\text{XZ planes}} E_+ [\hat{\rho}]_{\iota}^{+\text{xz}} - \sum_{c=\text{cube}} E_{\text{cube}} [\hat{\rho}]_c^{\text{cube}}$$

Thus, we are relabeling the σ and τ -links, but on the shared-links we are projecting into the $\tilde{\sigma}_{\ell}^x \tilde{\tau}_{\ell}^x = 1$ subspace. A hat over operators is used to denote operators in this new basis. See Fig. 6 and Fig. 7 for descriptions of the operators in $\hat{H}_{\text{X-cube}}$. In this basis, $\hat{H}_{\text{X-cube}}$ almost exactly reproduces the X-cube model introduced in [1]. The only difference is that $\hat{H}_{\text{X-cube}}$ does not include the $[\hat{\rho}]_{\iota}^{+\text{yz}} \equiv [\hat{\rho}]_{\iota}^{+\text{xy}} [\hat{\rho}]_{\iota}^{+\text{xz}}$ operator. However, this does not change the phase

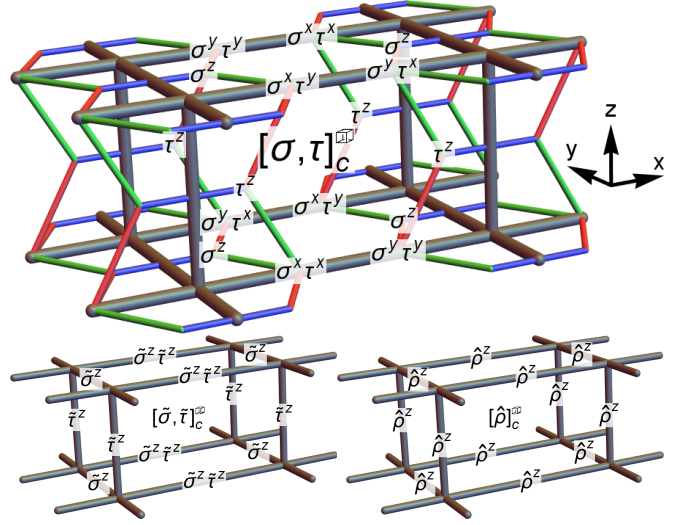


FIG. 6. The Z_2 fracton number operator generated from degenerate perturbation theory (Eq. (12)) when $\max(K_x, K_y) \ll \min(K_z, t)$. The operator is expressed in three different basis: $[\sigma, \tau]_c^{\text{cube}}$ is in original basis (Eq. (1)), $[\tilde{\sigma}, \tilde{\tau}]_c^{\text{cube}}$ is in the 2D toric code basis (Eq. (5)), and $[\hat{\rho}]_c^{\text{cube}}$ is in the X-cube model basis (Eq. (14)). $[\tilde{\sigma}, \tilde{\tau}]_c^{\text{cube}}$ is the product of two XY-plane and two XZ-plane plaquette/flux operators ($[\tilde{\sigma}]_p^{\square xy}$ and $[\tilde{\tau}]_p^{\square xz}$, Fig. 4) around the cube.

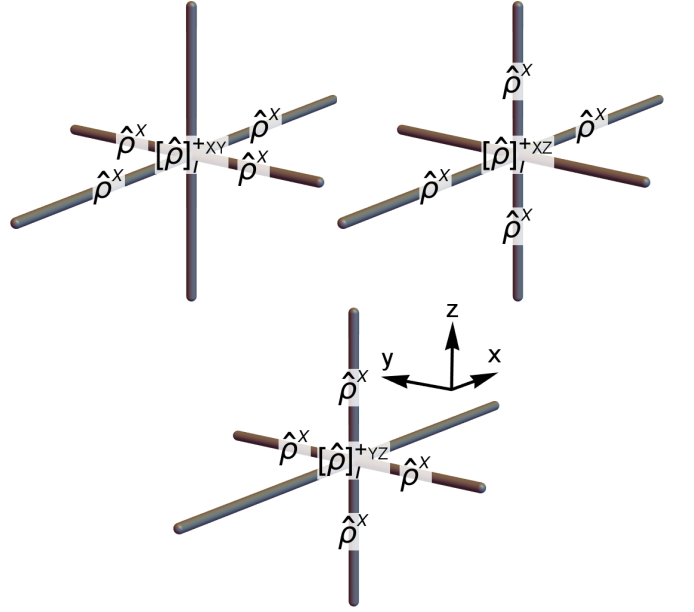


FIG. 7. The $[\hat{\rho}]_{\iota}^{+\text{xy}}$, $[\hat{\rho}]_{\iota}^{+\text{xz}}$, and $[\hat{\rho}]_{\iota}^{+\text{yz}}$ operators in the X-cube basis (Eq. (14)). These operators, along with $[\hat{\rho}]_c^{\text{cube}}$ (Fig. 6), are the commuting operators used to define the X-cube fracton Hamiltonian (Eq. (12)) after a change of basis (14). $[\sigma]_{\iota}^{+\text{xy}}$ was given in the original basis in Fig. 4; $[\tau]_{\iota}^{+\text{xz}}$ is similar, but with $\sigma \leftrightarrow \tau$ and on a XZ plane instead of a XY plane. $[\sigma, \tau]_{\iota}^{+\text{yz}}$ is given by $[\sigma, \tau]_{\iota}^{+\text{yz}} = [\sigma]_{\iota}^{+\text{xy}} [\tau]_{\iota}^{+\text{xz}}$.

of the Hamiltonian; it merely adds anisotropy. Only two of $[\hat{\rho}_\ell^{+xy}]$, $[\hat{\rho}_\ell^{+xz}]$, and $[\hat{\rho}_\ell^{+yz}]$ are necessary for X-cube order, since the third is a product of the other two. Therefore, when $\max(K_x, K_y) \ll \min(K_z, t)$, our model (Eq. (1)) has X-cube fracton topological order, as claimed in the phase diagram Fig. 3. Note that $\tilde{H}_{\text{X-cube}}$ is actually a rather simple Hamiltonian in the sense that all of its terms commute. Its ground state is specified by $[\hat{\rho}_\ell^{+xy}] = [\hat{\rho}_\ell^{+xz}] = [\hat{\rho}_c^{\text{op}}] = 1$ and has degeneracy 2^{6L-3} on a 3D torus [1, 18]. It is also interesting to note that the X-cube operators generated by DPT ($[\sigma, \tau]_p^{\text{op}}$, $[\sigma]_\ell^{+xy}$ and $[\tau]_\ell^{+xz}$) all commute with the original Hamiltonian (Eq. (1)).

$[\hat{\rho}_c^{\text{op}}]$ is the fracton number operator. Its excitations are of particular interest because they can only be created in groups of four [1, 9]. This can be seen from Fig. 6 where the application of a single $\hat{\rho}_\ell^x$ operator on any link ℓ will excite four $[\hat{\rho}_c^{\text{op}}]$ fracton operators on the four cubes that share the link ℓ . If we have an isolated fracton, then due to the Z_2 nature of the fracton operator, the application of a $\hat{\rho}_\ell^x$ operator will annihilate the isolated fracton but create three other fractons. Therefore, an isolated fracton can not move without creating additional excitations. An isolated fracton is immobile; only a pair of fractons can move without creating additional excitations.

III. DUALITY AND PHASE TRANSITIONS OUT OF X-CUBE ORDER

A. 2+1D Duality

In this subsection we will discuss a duality (similar to the one in Ref. [17], see Sec. IV D for connections) which describes a (likely first order) phase transition from X-cube fracton order to decoupled XY&XZ plane 2+1D Z_2 topological order. The duality will be applied to \tilde{H} (Eq. (8)):

$$\begin{aligned} \tilde{H} &= \tilde{H}_{\text{toric}} + \tilde{H}_t \\ &\sim -E_{\square} ([\tilde{\sigma}]_p^{\square xy} + [\tilde{\tau}]_p^{\square xz}) - E_{+} ([\tilde{\sigma}]_\ell^{+xy} + [\tilde{\tau}]_\ell^{+xz}) \\ &\quad - t \tilde{\sigma}_\ell^x \tilde{\tau}_\ell^x \end{aligned} \quad (16)$$

The last line above is just a short-hand representation of \tilde{H} , and is only shown for convenience.

Recall that \tilde{H}_{toric} (Eq. (6)) describes decoupled stacks of 2+1D toric codes along the XY and XZ planes. (The tilde over operators is still used to distinguish from the Pauli operators in the original Hamiltonian (Eq. (1)).) The XY-plane toric codes are composed of Pauli operators $\tilde{\sigma}_\ell^\mu$ on the links of the XY-plane square lattices, and are described by plaquette/flux operators $[\tilde{\sigma}]_p^{\square xy}$ and vertex/charge operators $[\tilde{\sigma}]_\ell^{+xy}$ (Fig. 4). The XZ-plane toric codes are similar, but are defined using $\tilde{\tau}$ instead of $\tilde{\sigma}$. The XY and XZ-plane toric code square lattices intersect on the links parallel to the x-axis, which

we have previously referred to as shared-links. \tilde{H}_t induces X-cube order at large t by coupling these shared-links together via a $t \tilde{\sigma}_\ell^x \tilde{\tau}_\ell^x$ coupling.

First, note that that $[\tilde{\sigma}]_\ell^{+xy}$, $[\tilde{\tau}]_\ell^{+xz}$, and $[\tilde{\sigma}, \tilde{\tau}]_c^{\text{op}}$ all commute with \tilde{H} . Recall that $[\tilde{\sigma}, \tilde{\tau}]_c^{\text{op}}$ is the product of two XY-plane and two XZ-plane flux operators ($[\tilde{\sigma}]_p^{\square xy}$ and $[\tilde{\tau}]_p^{\square xz}$) that boarder the cube c . (Note, there are no YZ-plane flux operators on the other two faces of the cube.) Therefore, we can work in the restricted Hilbert space where

$$[\tilde{\sigma}]_\ell^{+xy} |\Psi\rangle = [\tilde{\tau}]_\ell^{+xz} |\Psi\rangle = [\tilde{\sigma}, \tilde{\tau}]_c^{\text{op}} |\Psi\rangle = |\Psi\rangle \quad (17)$$

This is similar to imposing a charge-free gauge constraint when one considers dualities of pure Z_2 gauge theory. For example, our restricted Hilbert space does not allow any fracton excitations, which are excitations of $[\tilde{\sigma}, \tilde{\tau}]_c^{\text{op}}$.

The dual theory will consist of a stack of decoupled YZ-plane square lattices with vertices \hat{i} at the center of the x-axis links ℓ of the original cubic lattice. We introduce a new Pauli operator η_ℓ^μ which lives on the dual lattice vertices (Fig. 1 (b)). η_ℓ^μ will only be coupled along YZ planes; different YZ planes will be completely decoupled from each other. The duality is given by

$$\begin{aligned} [\tilde{\sigma}]_p^{\square xy} &\leftrightarrow \eta_{\hat{i}}^z \eta_{\hat{i}'}^z \\ [\tilde{\tau}]_p^{\square xz} &\leftrightarrow \eta_{\hat{i}}^z \eta_{\hat{i}'}^z \quad \text{where } \hat{i} \text{ and } \hat{i}' \text{ boarder } p \\ \tilde{\sigma}_\ell^x \tilde{\tau}_\ell^x &\leftrightarrow \eta_{\hat{i}=\ell}^x \\ [\tilde{\sigma}]_\ell^{+xy} &\leftrightarrow 1 \\ [\tilde{\tau}]_\ell^{+xz} &\leftrightarrow 1 \\ [\tilde{\sigma}, \tilde{\tau}]_c^{\text{op}} &\leftrightarrow 1 \end{aligned} \quad (18)$$

Therefore, the flux (XY plane $[\tilde{\sigma}]_p^{\square xy}$ or XZ plane $[\tilde{\tau}]_p^{\square xz}$) through the plaquette p is mapped to $\eta_{\hat{i}}^z \eta_{\hat{i}'}^z$, where \hat{i} and \hat{i}' reside at the center of the two x-axis links of the plaquette p . The coupling $\tilde{\sigma}_\ell^x \tilde{\tau}_\ell^x$ (on an x-axis link) is mapped to $\eta_{\hat{i}}^x$, which resides at the center of the link ℓ . $[\tilde{\sigma}]_\ell^{+xy}$, $[\tilde{\tau}]_\ell^{+xz}$, and $[\tilde{\sigma}, \tilde{\tau}]_c^{\text{op}}$ are mapped to the identity, which solves the Hilbert space constraint Eq. (17).

Note that the algebra (e.g. commutation relations) of the operators on the left hand side (LHS) and right hand side (RHS) of Eq. (18) are the same. Furthermore, the LHS and RHS both have exactly one effective qubit per unit cell. The LHS originally has 4 qubits (two $\tilde{\sigma}$ and two $\tilde{\tau}$), but this gets subtracted by 3 qubits due to the 3 restricted Hilbert space conditions (Eq. (17)). Therefore, the transformation (Eq. (18)) is an algebra isomorphism (on an infinite lattice) between the algebra of $\tilde{\sigma}_\ell^\mu$ and $\tilde{\tau}_\ell^\mu$ modulo the Hilbert space restriction (Eq. (17)), and the algebra of η_ℓ^μ . Thus, Eq. (18) is a valid duality transformation.

The dual Hamiltonian is described by decoupled 2+1D transverse field Ising models on the dual YZ-plane square

lattices:

$$\tilde{H}^{\text{dual}} = - \sum_{\langle i\tilde{i}' \rangle}^{\text{YZ planes}} E_{\square} \eta_i^z \eta_{\tilde{i}'}^z - \sum_i t \eta_i^x \quad (19)$$

$\sum_{\langle i\tilde{i}' \rangle}^{\text{YZ planes}}$ sums over nearest-neighbor dual lattice vertices that lie on the same YZ plane. We see that the decoupled phase (XY & XZ plane Z_2 topological order) with small coupling t is dual to the ordered phase of \tilde{H}^{dual} , and the X-cube phase with large t is dual to the disordered phase of \tilde{H}^{dual} .

In the original model \hat{H} (Eq. (16)), the t coupling, which couples together orthogonal layers of toric code, creates a YZ-plane loop of four fluxes (two XY and two XZ-plane fluxes: Fig. 1 (b)). In the previous subsection (Sec. II B) we use degenerate perturbation theory to show that at strong coupling, this YZ-plane composite flux loop condenses, and X-cube order results. Similar to the explanations in Ref. [17, 18], this occurs because the XY and XZ-plane toric code charge excitations ($[\tilde{\sigma}]_l^{+xy}$ and $[\tilde{\tau}]_l^{+xz}$) can no longer move in the x direction since they have nontrivial braiding statistics with the YZ-plane composite flux loop. Only a bound state of an XY and an XZ-plane toric code charge excitation can move in the x direction; but this composite particle can no longer move in any other direction. One can also consider a pair of open YZ-plane flux loop excitations, which have immobile fracton excitations $[\tilde{\sigma}, \tilde{\tau}]_c^{\text{op}}$ (Eq. (6)) at the open endpoints. Before the composite flux condensation, open flux loops have energy proportional to their length; however, after condensation, the bulk of the open flux loop is indistinguishable from the bulk of a closed flux loop, which carries no energy. Thus, arbitrarily long open YZ-plane flux loops only carry a finite energy cost at their boundaries. We see that in \tilde{H}^{dual} , the t coupling flips a η^z spin, which will either create or deform a domain wall on a YZ plane. Thus, the condensation of YZ-plane flux loops is dual to a proliferation of YZ-plane domain walls in 2+1D YZ-plane Ising models.

Although the spontaneous symmetry breaking phase transition of a single layer of the 2+1D transverse-field Ising model is continuous, the same transition for a stack of Ising models (i.e. \tilde{H}^{dual}) appears to be first order once they are weakly coupled. This is because a $\phi_L^2 \phi_{L'}^2$ term (in a stack of ϕ^4 field theories) or $\sigma_{LI}^z \sigma_{L'J}^z \sigma_{L'I}^z \sigma_{L'J}^z$ term (in a stack of transverse-field Ising models) is allowed by the subsystem symmetry, where L and L' denote different layers, and I and J are nearest-neighbor sites on a layer. ($\phi_L \phi_{L'}$ or $\sigma_{LI}^z \sigma_{L'I}^z$ are odd under subdimensional symmetry and thus not allowed.) ϕ^2 has scaling dimension ~ 1.4 , and thus $\phi_L^2 \phi_{L'}^2$ can be expected to have dimension $\sim 1.4 \times 2 \sim 2.8$, which is less than the dimension (2+1) of the critical Ising layers. Thus $\phi_L^2 \phi_{L'}^2$ is likely to be relevant under RG at the critical point, which implies that the transition of weakly coupled 2+1D Ising layers is not described

by the decoupled transition. According to the duality mapping (Eq. (18)), the relevant operator corresponds to a product of two $[\tilde{\sigma}]_p^{\square xy}$ or $[\tilde{\tau}]_p^{\square xz}$ operators. In Appendix C we provide classical Monte Carlo evidence that these symmetry allowed perturbations are relevant under RG, and that this transition and its dual are likely to be discontinuous and first order.

B. 1+1D Duality

In this subsection we will discuss a duality describing a (likely first order) phase transition from the X-cube phase to a phase of decoupled YZ-plane 2+1D Z_2 topological order. To do this, we will consider the X-cube model, but with a dimension-1 particle hopping term (and a perturbation):

$$\begin{aligned} \hat{H}_{\text{hop}} &= \hat{H}_{\text{X-cube}} - \sum_{\ell}^{\text{x-axis links}} h \hat{\rho}_{\ell}^z - \sum_{p=\square}^{\text{YZ planes}} E_{\square}^{\text{YZ}} [\hat{\rho}]_p^{\square yz} \\ \hat{H}_{\text{X-cube}} &= - \sum_{\iota=+}^{\text{XY planes}} E_{+} [\hat{\rho}]_{\iota}^{+xy} - \sum_{\iota=+}^{\text{XZ planes}} E_{+} [\hat{\rho}]_{\iota}^{+xz} \\ &\quad - \sum_{c=\text{op}} E_{\text{op}} [\hat{\rho}]_c^{\text{op}} \end{aligned} \quad (20)$$

where $\sum_{\ell}^{\text{x-axis links}}$ sums over all links ℓ which are parallel to the x-axis. The hopping term h (which we also consider in Sec. IV) hops the $[\hat{\rho}]_{\iota}^{+xy}$ and $[\hat{\rho}]_{\iota}^{+xz}$ excitations (Fig. 7) along the x-axis, which will condense the X-cube ordered phase into YZ-plane 2+1D Z_2 topological order. A small $E_{\square}^{\text{YZ}} [\hat{\rho}]_p^{\square yz}$ perturbation is included to prevent fine tuning, where $[\hat{\rho}]_p^{\square yz}$ is a YZ-plane toric code flux operator (Fig. 9). Similar to $H_{h'}$ (Eq. (27)) in a later section, without the E_{\square}^{YZ} term, the large h phase would have an unphysical degeneracy $\sim 2^{L^2}$ due to accidental symmetries which prevent a $[\hat{\rho}]_p^{\square yz}$ flux term from being generated. Terms other than $E_{\square}^{\text{YZ}} [\hat{\rho}]_p^{\square yz}$ can also work; however, this is the simplest choice for understanding the duality.

$\hat{H}_{\text{X-cube}}$ describes the X-cube model [1] with $\hat{\rho}^{\mu}$ operators on the links of a cubic lattice. (The hat over operators is used to distinguish them from the Pauli operators in the original Hamiltonian (Eq. (1) and previous section).) $[\hat{\rho}]_c^{\text{op}}$ (Fig. 6) measures the fracton number and is a product of the twelve $\hat{\rho}_{\ell}^z$ operators on the edges of the cube c . $[\hat{\rho}]_{\iota}^{+xy}$, $[\hat{\rho}]_{\iota}^{+xz}$, and $[\hat{\rho}]_{\iota}^{+yz} = [\hat{\rho}]_{\iota}^{+xy} [\hat{\rho}]_{\iota}^{+xz}$ (Fig. 7) are products of four $\hat{\rho}_{\ell}^x$ operators and correspond to dimension-1 particle excitations, which can only move along 1-dimensional lines. (The absence of $[\hat{\rho}]_{\iota}^{+yz}$ in $\hat{H}_{\text{X-cube}}$ is not important.)

$[\hat{\rho}]_{\iota}^{+yz}$ and $[\hat{\rho}]_c^{\text{op}}$ commute with \hat{H}_{hop} (Eq. (20)), and therefore we can work in a restricted Hilbert space where

$$[\hat{\rho}]_{\iota}^{+yz} |\Psi\rangle = [\hat{\rho}]_c^{\text{op}} |\Psi\rangle = |\Psi\rangle \quad (22)$$

The dual theory will consist of a grid of weakly coupled Ising chains along the x-axis with the same lattice sites ι as the original cubic lattice. We introduce a new Pauli operator μ_ι^α which lives on the vertices of the cubic lattice. The duality is given by

$$\begin{aligned}
[\hat{\rho}]_\iota^{+xy} &\leftrightarrow \mu_\iota^x \\
[\hat{\rho}]_\iota^{+xz} &\leftrightarrow \mu_\iota^x \\
[\hat{\rho}]_\iota^{+yz} &\leftrightarrow 1 \\
\hat{\rho}_\ell^z &\leftrightarrow \mu_\ell^z \mu_{\ell'}^z, \quad \text{for x-axis link } \ell = \langle \iota \iota' \rangle \\
[\hat{\rho}]_p^{\square yz} &\leftrightarrow \prod_{\iota \in \square} \mu_\iota^z \\
[\hat{\rho}]_c^{\text{op}} &\leftrightarrow 1
\end{aligned} \tag{23}$$

Thus, the dimension-1 particle ($[\hat{\rho}]_\iota^{+xy}$ and $[\hat{\rho}]_\iota^{+xz}$) number operator is mapped to a spin flip operator μ_ι^x ; and the dimension-1 particle hopping $\hat{\rho}_\ell^z$ is mapped to a domain wall number operator $\mu_\ell^z \mu_{\ell'}^z$. $[\hat{\rho}]_\iota^{+yz}$ and $[\hat{\sigma}, \hat{\tau}]_c^{\text{op}}$ are mapped to the identity, which solves the Hilbert space constraint Eq. (22). The YZ-plane flux operator $[\hat{\rho}]_p^{\square yz}$ is mapped to a product of four μ_ι^z operators at the corners of the plaquette p . The duality mapping forms an algebra isomorphism (on an infinite lattice) of the left hand side (LHS) of Eq. (23) (modulo the Hilbert space restriction (Eq. (22))), and the right hand side (RHS). For example, both the LHS and RHS have one effective qubit per unit cell. The LHS originally has 3 qubits ($\hat{\rho}_\ell^\mu$ along the three different directions), but this gets subtracted by 2 qubits due to the 2 Hilbert space conditions (Eq. (22)).

The dual Hamiltonian is described by a grid of 1+1D transverse field Ising models parallel to the x-axis (Fig. 1 (c)):

$$\begin{aligned}
\hat{H}_{\text{hop}}^{\text{dual}} = & - \sum_{\iota} (2E_+ \mu_\iota^x + h \mu_\iota^z \mu_{\iota+\hat{x}}^z \\
& + E_{\square}^{\text{YZ}} \mu_\iota^z \mu_{\iota+\hat{y}}^z \mu_{\iota+\hat{z}}^z \mu_{\iota+\hat{y}+\hat{z}}^z)
\end{aligned} \tag{24}$$

We see that the X-cube phase with small hopping h is dual to the disordered phase of $\hat{H}_{\text{hop}}^{\text{dual}}$, and the YZ-plane topological order phase with large h is dual to the ordered phase of $\hat{H}_{\text{hop}}^{\text{dual}}$.

In the original model \hat{H}_{hop} (Eq. (20)), the h hopping hops dimension-1 particles (a composite excitation of $[\hat{\rho}]_\iota^{+xy}$ and $[\hat{\rho}]_\iota^{+xz}$) parallel to the x-axis. For large hopping strength h , these x-axis particles condense, and YZ-plane 2+1D Z_2 topological order results. This is shown in a latter section (Sec. IV B) using degenerate perturbation theory with a more general model including a t term, which is taken to be zero in this section. We now give a physical explanation. The x-axis particle condensation confines fracton excitations which are created by YZ-plane membrane operators, since these membrane operators have nontrivial statistics with the x-axis particle. This condensation also allows the y-axis

particle $[\hat{\rho}]_\iota^{+xy}$ to move along the z direction, since it can do this by splitting up into a z-axis particle (which can move in the z direction) and an x-axis particle, which costs no energy after its condensation. Thus, the y-axis and z-axis particles become YZ-plane toric code charge excitations. Therefore, after the x-axis particle condensation, there are no dimension-1 particles, which implies that the fracton excitations created by XY and XZ-plane membrane operators are no longer finite energy excitations. To understand this, note that in the X-cube phase, there is no excitation (with a nontrivial braiding statistic) that can be braided through the membrane along a small closed loop. However, after the x-axis particles are condensed and YZ-plane toric code charge excitations are permitted, the YZ-plane charge excitations can braid through an XY-plane membrane. As a result, an XY-plane (or XZ-plane) membrane will have an energy cost proportional to the number of YZ-plane charges that can braid around it, which is proportional to the length of the membrane in the x direction. Mathematically, this energy cost results from the YZ-plane toric code flux term $E_{\square}^{\text{YZ}} [\hat{\rho}]_p^{\square yz}$ in \hat{H}_{hop} (Eq. (20)). (The same physics explains why flux loops in 3+1D toric code have energy cost proportional to their length.) However, an XY-plane (or XZ-plane) membrane operator with small length (e.g. =1) in the x direction will have a finite energy cost; these operators create composite fracton excitations which are free to move along a YZ plane. After the x-axis particles condense, this composite fracton excitation becomes the YZ-plane toric code flux excitation.

In the dual theory $\hat{H}_{\text{hop}}^{\text{dual}}$, h hops excitations of the spin flip operator μ_ι^x , which spontaneously breaks Z_2 Ising symmetry when condensed since these excitations are conserved modulo two due to the Z_2 Ising symmetry. The E_{\square}^{YZ} term couples four neighboring 1+1D chains together, which is a marginal under RG operator at the Ising phase transition. This can be understood by mapping the Ising chains to free Majorana chains using a Jordan-Wigner transformation; the E_{\square}^{YZ} term is then mapped to a mass-mass term $(\chi_\iota^T \sigma^2 \chi_\iota)(\chi_{\iota'}^T \sigma^2 \chi_{\iota'})$. Since $\chi_\iota^T \sigma^2 \chi_\iota$ has scaling dimension 1, the E_{\square}^{YZ} term has scaling dimension 2×1 , which is equal to the number of space-time dimensions of each chain (1+1). Thus, the E_{\square}^{YZ} term is marginal under RG at the fixed point of critical decoupled Ising chains. In Appendix C we show classical Monte Carlo evidence that these symmetry allowed perturbations are likely to be relevant under RG, and that this transition and its dual are likely to be discontinuous and first order.

In the next section, we introduce an extended honeycomb-based model H' (Eq. (25)) which also exhibits this phase transition with a similar duality description at low energies.

IV. EXTENDED MODEL WITH 3+1D Z_2 TOPOLOGICAL ORDER

To induce 3+1D Z_2 topological order instead of fracton order, we can consider adding to $H = H_K + H_t$ (Eq. (1)) a coupling H_h and a small perturbation, for which we will choose $H_{h'}$ as an example:

$$H' = H_K + H_t + H_h + H_{h'} \quad (25)$$

$$H_h = - \sum_{\langle ij \rangle}^{\text{shared-links}} \frac{h}{4} (\sigma_i^x \sigma_j^y + \sigma_i^y \sigma_j^x) (\tau_i^x \tau_j^y + \tau_i^y \tau_j^x) \quad (26)$$

$$H_{h'} = - \sum_i^{\sigma\text{-sites}} \frac{h'}{2} \sigma_i^z - \sum_i^{\tau\text{-sites}} \frac{h'}{2} \tau_i^z \quad (27)$$

A rough phase diagram for this model is given in Fig. 8. See Sec. IV D for connections to previous work.

H_h is an alternative coupling of the 2D honeycomb lattices. $\sum_{\langle ij \rangle}^{\text{shared-links}}$ sums over all shared links. As we will explain in Sec. IV A, this term will cause a composite charge excitation to condense, resulting in a phase which is fine tuned (with unphysical degeneracy $\sim 2^{L^2}$ on a torus). When generic perturbations are added (e.g. h'), the resulting phase is 3+1D Z_2 topological order.

$H_{h'}$ will be considered as an example of a generic perturbation to break the unphysical degeneracy mentioned in the previous paragraph. The particular choice of $H_{h'}$ is not important.

In the tilde basis (which includes a low energy Hilbert space projection from degenerate perturbation theory), H' is given by (ignoring subleading terms)

$$H' \rightarrow \tilde{H}' = \tilde{H}_{\text{toric}} + \tilde{H}_t + \tilde{H}_h + \tilde{H}_{h'} \quad (28)$$

$$H_h \rightarrow \tilde{H}_h = - \sum_{\ell}^{\text{shared-links}} h \tilde{\sigma}_{\ell}^z \tilde{\tau}_{\ell}^z \quad (29)$$

$$H_{h'} \rightarrow \tilde{H}_{h'} = - \sum_{\ell}^{\sigma\text{-links}} h' \tilde{\sigma}_{\ell}^z - \sum_{\ell}^{\tau\text{-links}} h' \tilde{\tau}_{\ell}^z \quad (30)$$

\tilde{H}_{toric} (Eq. (6)) and \tilde{H}_t (Eq. (9)) were discussed previously. We see that \tilde{H}_h couples the XY and XZ-toric codes together on the shared-links with a $\tilde{\sigma}_{\ell}^z \tilde{\tau}_{\ell}^z$ coupling. If $\ell = \langle \iota \iota' \rangle$ is a cubic lattice link between vertices ι and ι' , then when acting on the decoupled $t = h = 0$ ground state, $\tilde{\sigma}_{\ell}^z \tilde{\tau}_{\ell}^z$ creates the following four excitations: $[\tilde{\sigma}_{\iota}^+]^{+xy}$, $[\tilde{\sigma}_{\iota'}^+]^{+xy}$, $[\tilde{\tau}_{\iota}^+]^{+xz}$, $[\tilde{\tau}_{\iota'}^+]^{+xz}$. When t is small and h is large (and h' is small but finite), these excitations condense and the result is 3+1D Z_2 topological order.

A. 3+1D Z_2 Topological Order

In this section, we will explain how 3+1D Z_2 topological order results from H' (Eq. (25)) in the limit

$$\max(K_x, K_y) \ll h \ll K_z \quad \text{and } t = 0 \quad (31)$$

phase diagram $\max(K_x, K_y) \ll K_z$

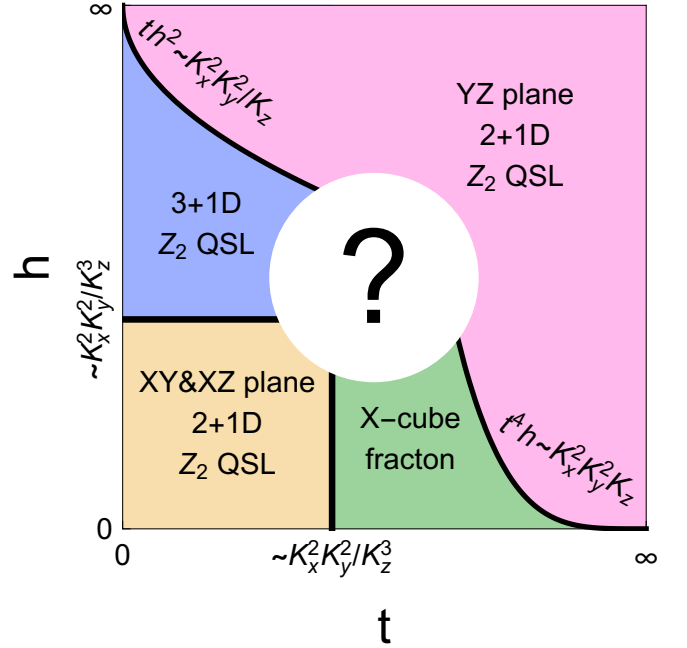


FIG. 8. Rough phase diagram of H' (Eq. (25)) as a function of t (horizontal axis) and h (vertical axis) in the limit $\max(K_x, K_y) \ll K_z$ with $\max(K_x, K_y)/K_z$ small but finite and h' infinitesimally small (to break accidental degeneracies). In Fig. 11 we utilize infinitesimal $\max(K_x, K_y)/K_z$ in order to display more precise claims regarding phase boundaries. Rough phase boundaries are computed in Appendix A. Four phase transitions occur around the edge of the phase diagram. In Sec. III and Sec. IV C we present dual descriptions of these four (likely first order) phase transitions. We do not know what phase(s) occur in the white region; this “region of ignorance” grows as we move away from the $\max(K_x, K_y) \ll K_z$ limit. In Appendix C we find that (depending on the sign of certain perturbations) topologically ordered intermediate phases are also possible in between all of the above phase transitions.

and with infinitesimal h' (to break accidental degeneracies). In Appendix A 3 we will consider more general limits. However, $\max(K_x, K_y) \ll h \ll K_z$ allows us to apply the results from Sec. II A and is closely connected to the previous layer constructions in Ref. [17, 18], and so we will discuss this limit here.

Again, we will derive this result using degenerate perturbation theory (DPT). First, we split H' (Eq. (25)) into

$$\begin{aligned} H' &\approx H_0 + H_1 \\ H_0 &= \tilde{H}_h \\ H_1 &= \tilde{H}_{\text{toric}} + \tilde{H}_{h'} \end{aligned} \quad (32)$$

where \tilde{H}_{toric} (Eq. (6)) describes the decoupled toric codes

on XY and XZ planes. Eq. (31) is sufficient to ensure that DPT converges. $[\tilde{\sigma}]_p^{\square xy}$ and $[\tilde{\tau}]_p^{\square xz}$ (in \tilde{H}_{toric}) commute with $H_0 = \tilde{H}_h$, and will therefore appear in the effective Hamiltonian H^{eff} . These operators will play the role of flux operators on XY and XZ planes in 3+1D toric code. However, $[\tilde{\sigma}]_l^{+xy}$ and $[\tilde{\tau}]_l^{+xz}$ will not appear in H^{eff} since they do not commute with H_0 , which means that they create excitations out of the low energy Hilbert space. However, their product $[\tilde{\sigma}, \tilde{\tau}]_l^* \equiv [\tilde{\sigma}]_l^{+xy} [\tilde{\tau}]_l^{+xz}$ does commute with H_0 and will indeed appear in H^{eff} . In a new basis, $[\tilde{\sigma}, \tilde{\tau}]_l^*$ will take the form of a charge operator in 3+1D toric code. Thus, DPT will produce the following effective Hamiltonian

$$\begin{aligned}
H^{\text{eff}} &= \tilde{H}_{\text{3D toric}} + \dots \\
\tilde{H}_{\text{3D toric}} &= - \sum_{p=\square}^{\text{XY planes}} E_{\square} [\tilde{\sigma}]_p^{\square xy} - \sum_{p=\square}^{\text{XZ planes}} E_{\square} [\tilde{\tau}]_p^{\square xz} \\
&\quad - \sum_{p=\square}^{\text{YZ planes}} E_{\square}^{YZ} [\tilde{\sigma}, \tilde{\tau}]_p^{\square yz} - \sum_{l=*} E_* [\tilde{\sigma}, \tilde{\tau}]_l^*
\end{aligned} \tag{33}$$

$$E_* \sim \frac{E_+^2}{h} \sim \frac{K_x^4 K_y^4}{K_z^6 h} \quad (\text{assuming (31)})$$

$$[\tilde{\sigma}, \tilde{\tau}]_l^* \equiv [\tilde{\sigma}]_l^{+xy} [\tilde{\tau}]_l^{+xz} \tag{34}$$

$[\tilde{\sigma}, \tilde{\tau}]_p^{\square yz}$ is defined in Fig. 9

(Actually, two applications of DPT are necessary to generate $E_{\square}^{YZ} [\tilde{\sigma}, \tilde{\tau}]_p^{\square yz}$, as is done in Appendix A 3; this term will be explained soon.) Again, we perform a change of basis and projection into the low energy Hilbert space where now the energy of H_0 is minimized with $\tilde{\sigma}_{\ell}^z \tilde{\tau}_{\ell}^z = 1$ on every shared-link:

$$\begin{aligned}
\sigma\text{-links:} & \quad \tilde{\sigma}_{\ell}^{\mu} \rightarrow \hat{\rho}_{\ell}^{\mu} \\
\tau\text{-links:} & \quad \tilde{\tau}_{\ell}^{\mu} \rightarrow \hat{\rho}_{\ell}^{\mu} \\
\text{shared-links:} & \quad \tilde{\sigma}_{\ell}^z \tilde{\tau}_{\ell}^z \rightarrow 1 \\
& \quad \tilde{\sigma}_{\ell}^z \rightarrow \hat{\rho}_{\ell}^z \\
& \quad \tilde{\sigma}_{\ell}^x \tilde{\tau}_{\ell}^x \rightarrow \hat{\rho}_{\ell}^x
\end{aligned} \tag{35}$$

$$\begin{aligned}
\tilde{H}_{\text{3D toric}} &\rightarrow \hat{H}_{\text{3D toric}} \\
&= - \sum_{p=\square}^{\text{XY planes}} E_{\square} [\hat{\rho}]_p^{\square xy} - \sum_{p=\square}^{\text{XZ planes}} E_{\square} [\hat{\rho}]_p^{\square xz} \\
&\quad - \sum_{p=\square}^{\text{YZ planes}} E_{\square}^{YZ} [\hat{\rho}]_p^{\square yz} - \sum_{l=*} E_* [\hat{\rho}]_l^*
\end{aligned} \tag{36}$$

A hat over operators is also used to denote operators in this basis. In this basis, $\hat{H}_{\text{3D toric}}$ has the exact same form as 3+1D toric code, which has 3+1D Z_2 topological order.

However, we have not yet discussed the $E_{\square}^{YZ} [\tilde{\sigma}, \tilde{\tau}]_p^{\square yz}$ term in $\tilde{H}_{\text{3D toric}}$. In the new basis (Eq. (35)), $[\hat{\rho}]_p^{\square yz}$

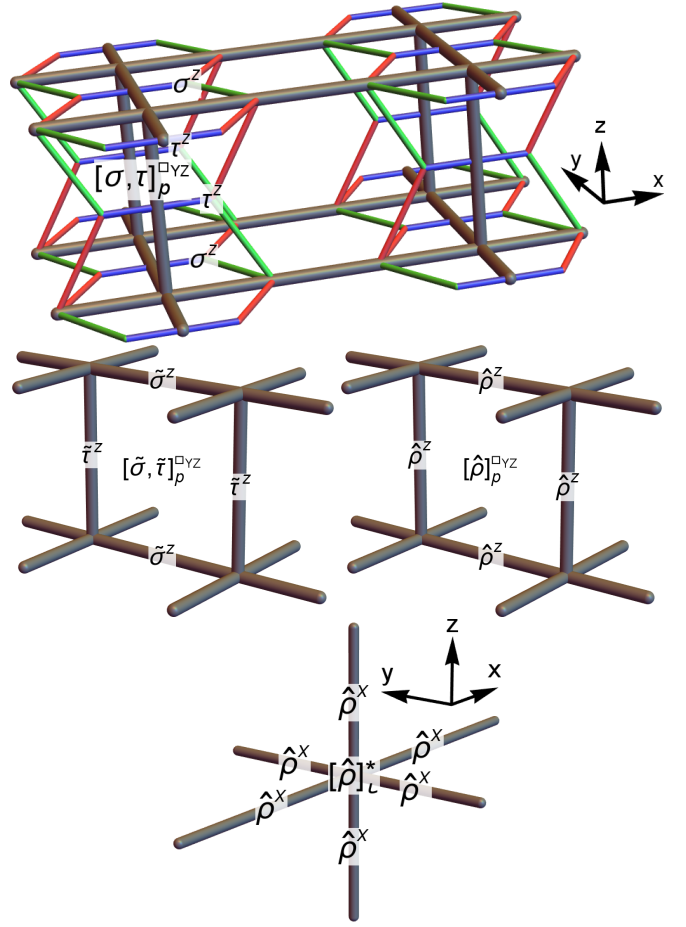


FIG. 9. The YZ-plane toric code plaquette/flux operator expressed in three different basis: $[\sigma, \tau]_p^{\square yz}$ (top) is in the original basis (Eq. (1)), $[\tilde{\sigma}, \tilde{\tau}]_p^{\square yz}$ (mid-left) is in the 2D toric code basis (Eq. (5)), and $[\hat{\rho}]_p^{\square yz}$ (mid-right) is the X-cube basis (Eq. (14)). $[\hat{\rho}]_l^*$ (bottom) is the vertex/charge operator in 3+1D toric code (Eq. (33)).

takes the form of a flux operator on YZ planes in 3+1D toric code. This term is necessary in 3+1D toric code; without it, $\tilde{H}_{\text{3D toric}}$ would have an unphysical degeneracy $\sim 2^{L^2}$ on a 3D torus. But without $H_{h'}$, $[\tilde{\sigma}, \tilde{\tau}]_p^{\square yz}$ can not be generated by DPT (due to accidental symmetries). Therefore, we add an infinitesimal perturbation $H_{h'}$ to break this degeneracy. The choice of perturbation is not important, and we only choose $H_{h'}$ as a simple example. Most sufficiently general and sufficiently small perturbations will generate $[\tilde{\sigma}, \tilde{\tau}]_p^{\square yz}$ and not affect the resulting phase.

B. YZ Plane 2+1D Z_2 Topological Order

In this section, we will explain why 2+1D Z_2 topological order on YZ planes results from H' (Eq. (25))

in the limit

$$\max(K_x, K_y) \ll \min(t, h) \text{ and } \max(t, h) \ll K_z \quad (37)$$

with infinitesimal h' (to break accidental degeneracies). This phase is the same as a stack of decoupled toric codes on YZ planes. In the Appendix A 4 we will consider limits more general than Eq. (37). Starting again from the decoupled $t = h = 0$ limit discussed in Sec. II A, we make both h and t very large and perform DPT on \tilde{H}' (Eq. (28)). \tilde{H}_t (Eq. (9)) and \tilde{H}_h (Eq. (29)) couple the XY and XZ-plane toric codes together on the shared-links with $\tilde{\sigma}_\ell^x \tilde{\tau}_\ell^x$ and $\tilde{\sigma}_\ell^z \tilde{\tau}_\ell^z$ couplings. When acting on the decoupled $t = h = 0$ ground state, these couplings create toric code charge and flux excitations, and when t and h are large, these excitations condense and the result is 2+1D Z_2 topological order on YZ planes.

To understand this, we again apply degenerate perturbation theory (DPT) by splitting H' (Eq. (25)) into

$$\begin{aligned} H' &\approx H_0 + H_1 \\ H_0 &= \tilde{H}_t + \tilde{H}_h \\ H_1 &= \tilde{H}_{\text{toric}} + H_{h'} \end{aligned} \quad (38)$$

Eq. (37) is sufficient to ensure that DPT converges. No operator in \tilde{H}_{toric} (Eq. (6)) will appear in H^{eff} since they do not commute with H_0 ; i.e. they create excitations out of the low energy Hilbert space. However, $[\tilde{\sigma}, \tilde{\tau}]_c^{\text{op}}$ and $[\tilde{\sigma}, \tilde{\tau}]_l^{+\text{YZ}}$ ($= [\tilde{\sigma}, \tilde{\tau}]_l^*$ from Eq. (34)) are generated by DPT, and the effective Hamiltonian is

$$\begin{aligned} H^{\text{eff}} &= \tilde{H}_{\text{toric}}^{\text{YZ}} - \sum_{c=\text{op}} E_{\text{op}} [\tilde{\sigma}, \tilde{\tau}]_c^{\text{op}} + \dots \\ \tilde{H}_{\text{toric}}^{\text{YZ}} &= - \sum_{p=\square}^{\text{YZ planes}} E_{\square}^{\text{YZ}} [\tilde{\sigma}, \tilde{\tau}]_p^{\square\text{YZ}} \\ &\quad - \sum_{\iota=+}^{\text{YZ planes}} E_{+}^{\text{YZ}} [\tilde{\sigma}, \tilde{\tau}]_{\iota}^{+\text{YZ}} \end{aligned} \quad (39)$$

$$\begin{aligned} E_{+}^{\text{YZ}} &\sim \frac{E_{+}^2}{h} \sim \frac{K_x^4 K_y^4}{K_z^6 h} \quad \text{assuming (37)} \\ E_{\text{op}} &\sim \frac{E_{\square}^4}{t^3} \sim \frac{K_x^8 K_y^8}{K_z^{12} t^3} \quad \text{assuming (37)} \end{aligned}$$

$$[\tilde{\sigma}, \tilde{\tau}]_l^{+\text{YZ}} \equiv [\tilde{\sigma}]_l^{+\text{XY}} [\tilde{\tau}]_l^{+\text{XZ}} \quad (40)$$

(Actually, two applications of DPT are necessary to generate $E_{+}^{\text{YZ}} [\tilde{\sigma}, \tilde{\tau}]_p^{\square\text{YZ}}$, as is done in Appendix A 4.) We perform a change of variables and projection into the low energy Hilbert space with $\tilde{\sigma}_\ell^x \tilde{\tau}_\ell^x = \tilde{\sigma}_\ell^z \tilde{\tau}_\ell^z = 1$ on every shared-link:

$$\begin{aligned} \sigma\text{-links:} & \quad \tilde{\sigma}_\ell^\mu \rightarrow \hat{\rho}_\ell^\mu \\ \tau\text{-links:} & \quad \tilde{\tau}_\ell^\mu \rightarrow \hat{\rho}_\ell^\mu \\ \text{shared-links:} & \quad \tilde{\sigma}_\ell^x \tilde{\tau}_\ell^x \rightarrow 1 \\ & \quad \tilde{\sigma}_\ell^z \tilde{\tau}_\ell^z \rightarrow 1 \end{aligned} \quad (41)$$

phase diagram

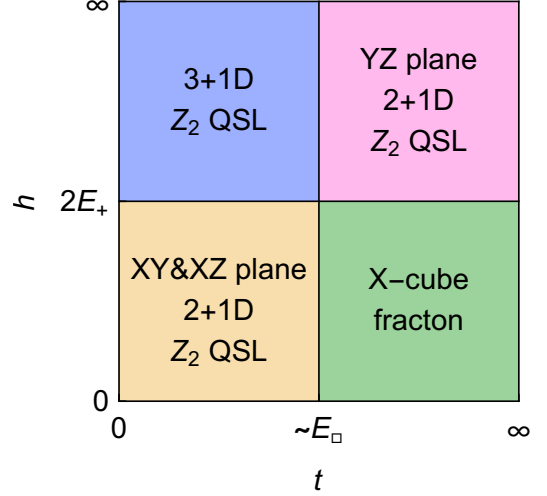


FIG. 10. Phase diagram of $\tilde{H}_{\text{global}}$ (Eq. (43)) for $E_{\square}^{\text{YZ}} \ll E_{+}$. $\tilde{H}_{\text{global}}$ is used to derive dual descriptions of the phase transitions between the above phases, which occur on the lines $t \sim E_{\square}$ and $h = 2E_{+}$. The phase boundaries in Fig. 8 are different because that phase diagram describes a model H' (Eq. (25)) where the effective E_{\square} and E_{+} depend on t and h as shown in Eq. (A1).

$$\tilde{H}_{\text{toric}}^{\text{YZ}} \rightarrow \hat{H}_{\text{toric}}^{\text{YZ}} \quad (42)$$

A hat over operators is also used to denote operators in this basis. In this basis, $\hat{H}_{\text{toric}}^{\text{YZ}}$ has the exact same form as decoupled 2+1D toric codes on YZ planes. $[\hat{\rho}]_l^{+\text{YZ}}$ and $[\hat{\rho}]_p^{\square\text{YZ}}$ are charge and flux operators on YZ planes in 2+1D toric code, respectively.

But just like $[\tilde{\sigma}, \tilde{\tau}]_p^{\square\text{YZ}}$ (Eq. (33)) in the previous section, $[\tilde{\sigma}, \tilde{\tau}]_p^{\square\text{YZ}}$ in Eq. (39) can not be generated from H' (Eq. (25)) with $h' = 0$. However, H' with $h' = 0$ does generate $[\tilde{\sigma}, \tilde{\tau}]_c^{\text{op}}$, which corresponds to a product of flux operators on neighboring YZ planes in the new basis (Eq. (42)); that is, $[\tilde{\sigma}, \tilde{\tau}]_c^{\text{op}} \rightarrow [\hat{\rho}]_c^{\text{op}} = [\hat{\rho}]_p^{\square\text{YZ}} [\hat{\rho}]_{p'}^{\square\text{YZ}}$ where YZ-plane plaquettes p and p' lie on the boundary of the cube c . Without perturbations such as $H_{h'}$, H^{eff} in Eq. (39) (and therefore also H') would have an unphysical degeneracy $\sim 2^{L^2}$ on a torus. Again, the choice of perturbation $H_{h'}$ is not important.

C. Global Duality of the Extended Model

In this subsection we discuss a global duality which describes the four (likely first order) phase transitions along the edge of Fig. 8. To do this, we merge \tilde{H}

(Eq. (16)) and \hat{H}_{hop} (Eq. (20)) from Sec. III:

$$\begin{aligned} \tilde{H}_{\text{global}} &= \tilde{H}_{\text{toric}} + \tilde{H}_t + \tilde{H}_h - \sum_{p=\square}^{\text{YZ planes}} E_{\square}^{\text{YZ}} [\tilde{\sigma}, \tilde{\tau}]_p^{\square\text{YZ}} \\ &\sim -E_{\square} ([\tilde{\sigma}]_p^{\square\text{XY}} + [\tilde{\tau}]_p^{\square\text{XZ}}) - E_+ ([\tilde{\sigma}]_l^{+\text{XY}} + [\tilde{\tau}]_l^{+\text{XZ}}) \\ &\quad - t \tilde{\sigma}_\ell^x \tilde{\tau}_\ell^x - h \tilde{\sigma}_\ell^z \tilde{\sigma}_\ell^z - E_{\square}^{\text{YZ}} [\tilde{\sigma}, \tilde{\tau}]_p^{\square\text{YZ}} \end{aligned} \quad (43)$$

$\tilde{H}_{\text{global}}$ is a model of XY and XZ-plane toric codes \tilde{H}_{toric} (Eq. (6)) which are coupled together by \tilde{H}_t (Eq. (9)) and \tilde{H}_h (Eq. (27)), with an infinitesimal perturbation $E_{\square}^{\text{YZ}} [\tilde{\sigma}, \tilde{\tau}]_p^{\square\text{YZ}}$ (Fig. 9) to break accidental degeneracies (discussed in Sec. III B, IV A, and IV B). \tilde{H}_{toric} and \tilde{H}_t were discussed in Sec. III A. \tilde{H}_h and $E_{\square}^{\text{YZ}} [\tilde{\sigma}, \tilde{\tau}]_p^{\square\text{YZ}}$ were discussed in Sec. III B in the X-cube basis (Eq. (14)); here we use the decoupled toric code basis (Eq. (5)). $\tilde{H}_{\text{global}}$ is very similar to \tilde{H}' (Eq. (28)); the only difference is that $\tilde{H}_{\text{global}}$ replaces $\tilde{H}_{h'}$ (Eq. (30)) with the E_{\square}^{YZ} term. (Recall that the choice of $\tilde{H}_{h'}$ in \tilde{H}' was not important.) $[\tilde{\sigma}]_p^{\square\text{XY}}$, $[\tilde{\sigma}]_l^{+\text{XY}}$ (Fig. 4), and $\tilde{\sigma}_\ell^x$ are defined on the XY plane toric codes, while $\tilde{\tau}$ operators are defined on XZ plane toric codes. The second line in Eq. (43) is just a short-hand representation of the included terms, and is only shown for convenience. A phase diagram is given in Fig. 10. We will work in a restricted Hilbert space where

$$[\tilde{\sigma}]_l^{+\text{XY}} [\tilde{\tau}]_l^{+\text{XZ}} |\Psi\rangle = [\tilde{\sigma}, \tilde{\tau}]_c^{\text{op}} |\Psi\rangle = |\Psi\rangle \quad (44)$$

The dual theory looks like a decoupled combination of the two dual theories discussed in Sec. III. Thus, the dual theory consists of a stack of decoupled YZ-plane square lattices with Pauli operators η_ℓ^α at vertices $\hat{\ell}$ centered on x-axis links ℓ of the original cubic lattice, and a grid of weakly coupled Ising chains along the x-axis with Pauli operators μ_ι^α on the same lattice sites ι as the original cubic lattice. η_ℓ^α and μ_ι^α will be completely decoupled. The duality is given by

$$\begin{aligned} [\tilde{\sigma}]_p^{\square\text{XY}} &\leftrightarrow \eta_\ell^z \eta_{\ell'}^z \\ [\tilde{\tau}]_p^{\square\text{XZ}} &\leftrightarrow \eta_\ell^z \eta_{\ell'}^z \quad \text{where } \hat{\ell} \text{ and } \hat{\ell}' \text{ boarder } p \\ \tilde{\sigma}_\ell^x \tilde{\tau}_\ell^x &\leftrightarrow \eta_{\hat{\ell}=\ell}^x \\ [\tilde{\sigma}]_l^{+\text{XY}} &\leftrightarrow \mu_\iota^x \\ [\tilde{\tau}]_l^{+\text{XZ}} &\leftrightarrow \mu_\iota^x \\ \tilde{\sigma}_\ell^z \tilde{\sigma}_\ell^z &\leftrightarrow \mu_\iota^z \mu_{\iota'}^z \quad \text{for x-axis link } \ell = \langle \iota \iota' \rangle \\ [\tilde{\sigma}, \tilde{\tau}]_p^{\square\text{YZ}} &\leftrightarrow \prod_{\iota \in p} \mu_\iota^z \\ [\tilde{\sigma}, \tilde{\tau}]_c^{\text{op}} &\leftrightarrow 1 \end{aligned} \quad (45)$$

The mapping is essentially a combination of the duality mappings in Sec. III: Eq. (18) and (23). Both the original theory (modulo the Hilbert space restriction (Eq. (44))) and the dual theory have two qubits per site. The dual

Hamiltonian is simply the decoupled sum of the two dual Hamiltonians in Sec. III (Eq. (19) and (24)):

$$\tilde{H}_{\text{global}}^{\text{dual}} = \tilde{H}^{\text{dual}} + \hat{H}_{\text{hop}}^{\text{dual}} \quad (46)$$

In Sec. III we described two phase transitions out of the X-cube order phase. $\tilde{H}_{\text{global}}^{\text{dual}}$ describes these transitions in the same way. We now explain how this duality also describes two transitions out of 3+1D Z_2 topological order.

Let us start in the XY & XZ plane Z_2 topological order phase with small t and h , and then increase h to transition into the 3+1D Z_2 topological order phase (Fig. 10). In the original model $\tilde{H}_{\text{global}}$ (Eq. (43)), the h coupling hops a composite excitation of XY and XZ-plane toric code charge excitations ($[\tilde{\sigma}]_l^{+\text{XY}}$ and $[\tilde{\tau}]_l^{+\text{XZ}}$, see Fig. 1 (c)). In Sec. IV A we used degenerate perturbation theory to show that for large hopping strength h , this composite charge excitation condenses, and 3+1D Z_2 topological order results. We now give a physical explanation. After the composite charge condenses, the XY and XZ-plane 2+1D toric code charge excitations are no longer bound to the XY and XZ planes (respectively) since an XY plane charge can split into a XZ plane charge and a composite charge excitation, which means that the XY and XZ-plane charges can freely transform into the other. A XY or XZ-plane charge excitation thus becomes a 3+1D toric code charge excitation after the composite charge condenses. Once the charges are no longer bound to planes, the XY and XZ-plane 2+1D toric code flux excitations are confined since they no longer have well defined braiding statistics with the charge excitations. That is, a pair of XY or XZ-plane flux excitations will incur an energy cost proportional to their distance due to two strings of YZ-plane toric code flux terms $E_{\square}^{\text{YZ}} [\tilde{\sigma}, \tilde{\tau}]_p^{\square\text{YZ}}$ which will also be excited. Thus, the XY and XZ-plane 2+1D toric code flux excitations become 3+1D toric code flux loop excitations when the composite charge condenses.

The dual theory is described by $\tilde{H}_{\text{global}}^{\text{dual}}$ (Eq. (46)). This transition is driven by increasing h (see Fig. 10) while keeping t constant. Since \tilde{H}^{dual} does not depend on h , and is completely decoupled from $\hat{H}_{\text{hop}}^{\text{dual}}$, the phase transition is just described by $\hat{H}_{\text{hop}}^{\text{dual}}$: i.e. decoupled 1+1D Ising chains. The composite charge excitation is dual to an excitation of the 1+1D Ising paramagnet (Fig. 1 (c)). Just like in Sec. III B, where a similar duality is discussed, $E_{\square}^{\text{YZ}} [\tilde{\sigma}, \tilde{\tau}]_p^{\square\text{YZ}}$ appears to be marginally relevant under RG (see Appendix C) at the phase transition, and the phase transition is likely first order. The extended honeycomb-based model (Eq. (25)) also exhibits this phase transition since $\tilde{H}_{\text{global}}$ (Eq. (43)) is the same as the effective Hamiltonian \tilde{H}' (Eq. (28)) of the honeycomb-based model in the $\max(K_x, K_y, t, h) \ll K_z$ limit (ignoring subleading terms), with the unimportant difference that $\tilde{H}_{\text{global}}$ includes $E_{\square}^{\text{YZ}} [\tilde{\sigma}, \tilde{\tau}]_p^{\square\text{YZ}}$ as a

perturbation, while \tilde{H}' instead includes \tilde{H}_h (Eq. (30)).

Let us now consider the 3+1D Z_2 topological order phase with small t and large h , and then increase t to transition into the YZ-plane Z_2 topological order phase (Fig. 10). In the original model $\tilde{H}_{\text{global}}$ (Eq. (43)), the t coupling creates a YZ-plane loop of four 3+1D toric code fluxes (Fig. 1 (b)). In Sec. IV B we used degenerate perturbation theory to show that for strong coupling t , the composite flux loops condense, and YZ-plane topological order results. This occurs because when the YZ-plane flux loops condense, the 3+1D toric code charge excitations can no longer move in the x direction, since this would incur a nontrivial braiding statistic with the condensed YZ-plane flux loops. Now consider an open flux loop excitation of 3+1D toric code that is long in the y and z directions, but very short in the x direction. Before the YZ-plane flux loops condense, this excitation has a large energy proportional to its length. However, after the YZ-plane flux loops condense, its bulk is indistinguishable to part of a YZ-plane flux loop, and therefore only a finite energy cost is incurred. Thus, the YZ-plane flux loop condensation allows 2+1D toric code flux excitations (at the end of the open flux loop) to become deconfined along the YZ plane.

The dual theory is described by decoupled YZ-plane 2+1D Ising models \tilde{H}^{dual} (Eq. (46)) since $\hat{H}_{\text{hop}}^{\text{dual}}$ does not depend on t . The YZ-plane flux loop excitation of $\tilde{H}_{\text{global}}$ is dual to a domain wall in a YZ-plane 2+1D Ising model (Fig. 1 (b)). Just like in Sec. III A, where a similar duality is discussed, this phase transition is also likely first order. The extended honeycomb-based model (Eq. (25)) also exhibits this phase transition since $\tilde{H}_{\text{global}}$ (Eq. (43)) is the same as the effective Hamiltonian \tilde{H}' (Eq. (28)) of the honeycomb-based model in the $\max(K_x, K_y, t, h) \ll K_z$ limit (ignoring subleading terms). This $\max(K_x, K_y, t, h) \ll K_z$ limit describes the phase transition out of 3+1D topological order across the vertical red line in 11. However, this $\max(K_x, K_y, t, h) \ll K_z$ limit does not correspond to the top-left corner of Fig. 8 for which $\max(K_x, K_y, t) \ll \min(K_z, h)$, which instead corresponds to the diagonal red on the top-left of 11. To describe the $\max(K_x, K_y, t) \ll \min(K_z, h)$ limit, we could apply a similar duality to the following Hamiltonian, which describes the extended honeycomb-based model (Eq. (25)) when $\max(K_x, K_y, t) \ll \min(K_z, h)$:

$$\hat{H}_{\text{coupled}} = \hat{H}_{\text{3D toric}} - \sum_{\ell}^{\text{x-axis links}} t \hat{\rho}_{\ell}^x \quad (47)$$

where $\hat{H}_{\text{3D toric}}$ is given in Eq. (36).

D. Connections to Previous Coupled Layer Constructions

$\tilde{H}_{\text{toric}} + \tilde{H}_t + \tilde{H}_h$ (Eq. (6), (9), and (30)) is very similar to the coupled layer constructions considered in Ref. [17] and [18]. The primary difference is that we have only XY and XZ-plane toric codes, while they also had YZ planes. This difference was motivated in our work by the desire to have the simplest possible lattice model. Although the lack of YZ planes in \tilde{H}_{toric} adds some anisotropy to the resulting X-cube Hamiltonian (Eq. (15)) and 3+1D toric code Hamiltonian (Eq. (36)), these details do not affect the universality class of these phases. However, when both t and h are large, the lack of YZ-plane toric codes in our model results in radically different physics. Specifically, in Sec. IV B we showed that XY and XZ-plane toric codes with large t and h coupling leads to a phase described by decoupled YZ-plane toric codes. However, with XY, XZ, and YZ planes, Ref. [17] showed that large t and h coupling drives the system into a trivial phase with no topological order. It is interesting that large t and h coupling seems to have a Z_2 action on the presence of topological order on YZ planes.

V. CONCLUSION

In this work we strive to bring the recently discovered fracton topological order closer to an experimental realization. We do this by presenting a simple model with X-cube fracton topological order which only requires nearest-neighbor 2-spin interactions. This is a significant improvement over the original X-cube model with 12-spin interactions [1], or previous coupled layer constructions with 4-spin interactions. Unfortunately however, it is likely that much future work will be necessary to realize fracton order in an experiment.

Perhaps there exists a material for which our model could be a useful description. If this is not the case, we hope that this work could be useful inspiration for deriving more realistic models of fracton order with possible experimental realizations. Additionally, synthetic quantum matter, such as cold atom experiments, provide another possible route to experimental realization. Perhaps previous theoretical work [20, 21] on synthetic quantum matter realizations of Kitaev's honeycomb model [2] could be generalized to apply to our model or to similar models. It would also be interesting to discover realistic models of other kinds of fracton order. In particular, it would be very interesting to realize fractal-like (type II in Ref. [1]) fracton topological order (e.g. Haah's code [7]) via a coupled layer construction or via a two-spin Hamiltonian.

In this work, we found two first order phase transitions out of the X-cube phase. Ref. [17] also showed that their isotropic coupled layer construction admits dualities

describing two first order phase transition out of X-cube fracton topological order. Additionally, Ref. [1] gave dualities describing phase transitions out of an entire class of fracton phases; however, the nature of these phase transitions is currently unknown. It remains an open and interesting question if it is possible to have a continuous phase transition out of fracton topological order.

In Fig. 8 and especially in Fig. 3, there are regions of the phase diagrams which could not be described by degenerate perturbation theory or the dualities that we found. In particular, it is not clear what occurs when K_x and K_y are increased above the $\max(K_x, K_y) \ll K_z$ limit in Fig. 3. A gapless version of X-cube fracton order would be an interesting possibility; however, such a phase is likely to be unstable to a gapped phase [17, 22]. It is also natural to ask what occurs near the center of Fig. 8.

It is also interesting to note that the X-cube operators that we generated using degenerate perturbation theory ($[\sigma, \tau]_p^{\text{op}}$ (Fig. 6), and $[\sigma]_l^{+xy}$ and $[\tau]_l^{+xz}$ (Fig. 4)) all commute with the original Hamiltonian (Eq. (1)). The original Hamiltonian has 8 qubit degrees of freedom for each unit cell; and we have found 3 qubit integrals of motion. In Kitaev's exactly solvable honeycomb model [2], every unit cell is comprised of 2 qubit degrees of freedom which are split into a single integral of motion given by a hexagon/vison operator (Fig. 4), and two Majorana fermions with only quadratic interactions for a given static configuration of hexagon/vison excitations. Perhaps our model, or a similar model, admits a similar exact solution, possibly with connections to the generalized parton constructions in Ref. [10].

Acknowledgements — We thank Leon Balents for pointing out the relevance of the layer couplings discussed in Appendix C. This work was supported by the NSERC of Canada and the Center for Quantum Materials at the University of Toronto. Computations were performed on the gpc supercomputer at the SciNet HPC Consortium. SciNet is funded by: the Canada Foundation for Innovation under the auspices of Compute Canada; the Government of Ontario; Ontario Research Fund - Research Excellence; and the University of Toronto. [23]

- (2015).
- [10] T. H. Hsieh and G. B. Halász, arXiv:1703.02973 [cond-mat, physics:quant-ph] (2017), arXiv:1703.02973 [cond-mat, physics:quant-ph].
- [11] A. Prem, J. Haah, and R. Nandkishore, arXiv:1702.02952 [cond-mat, physics:quant-ph] (2017), arXiv:1702.02952 [cond-mat, physics:quant-ph].
- [12] J. Haah, *Phys. Rev. B* **89**, 075119 (2014).
- [13] D. J. Williamson, *Phys. Rev. B* **94**, 155128 (2016).
- [14] M. Pretko, arXiv:1702.07613 [cond-mat, physics:gr-qc, physics:hep-th] (2017), arXiv:1702.07613 [cond-mat, physics:gr-qc, physics:hep-th].
- [15] S. Bravyi and J. Haah, *Phys. Rev. Lett.* **111**, 200501 (2013).
- [16] S. Bravyi and J. Haah, *Phys. Rev. Lett.* **107**, 150504 (2011).
- [17] S. Vijay, arXiv:1701.00762 [cond-mat] (2017), arXiv:1701.00762 [cond-mat].
- [18] H. Ma, E. Lake, X. Chen, and M. Hermele, arXiv:1701.00747 [cond-mat, physics:quant-ph] (2017), arXiv:1701.00747 [cond-mat, physics:quant-ph].
- [19] E. Dennis, A. Kitaev, A. Landahl, and J. Preskill, *Journal of Mathematical Physics* **43**, 4452 (2002), arXiv:quant-ph/0110143.
- [20] T. Tanamoto, K. Ono, Y.-x. Liu, and F. Nori, *Scientific Reports* **5**, 10076 (2015).
- [21] S. Liu and Z.-Y. Xue, *J. Opt. Soc. Am. B* **30**, 1720 (2013).
- [22] C. Xu and C. Wu, *Phys. Rev. B* **77**, 134449 (2008).
- [23] C. Loken, D. Gruner, L. Groer, R. Peltier, N. Bunn, M. Craig, T. Henriques, J. Dempsey, C.-H. Yu, J. Chen, L. J. Dursi, J. Chong, S. Northrup, J. Pinto, N. Knecht, and R. V. Zon, *Journal of Physics: Conference Series* **256**, 012026 (2010).
- [24] A. W. Sandvik, arXiv preprint arXiv:1101.3281 (2011).
- [25] J. R. Schrieffer and P. A. Wolff, *Phys. Rev.* **149**, 491 (1966).
- [26] S. Bravyi, D. P. DiVincenzo, and D. Loss, *Annals of Physics* **326**, 2793 (2011).
- [27] U. Wolff, *Phys. Rev. Lett.* **62**, 361 (1989).
- [28] K. Slagle, "MC," <https://github.com/kjstag/MC/tree/subdimensionalTransition> (2017).
- [29] The connected correlation length ξ_c was calculated using Eqn. 73 in [24].
- [30] K. Slagle, "degeneracy," <https://github.com/kjstag/degeneracy> (2017).

-
- [1] S. Vijay, J. Haah, and L. Fu, *Phys. Rev. B* **94**, 235157 (2016).
- [2] A. Kitaev, *Annals of Physics January Special Issue*, **321**, 2 (2006).
- [3] C. Chamon, *Phys. Rev. Lett.* **94**, 040402 (2005).
- [4] A. Rasmussen, Y.-Z. You, and C. Xu, arXiv:1601.08235 [cond-mat] (2016), arXiv:1601.08235 [cond-mat].
- [5] C. Xu, *Phys. Rev. B* **74**, 224433 (2006).
- [6] S. Bravyi, B. Leemhuis, and B. M. Terhal, *Annals of Physics* **326**, 839 (2011).
- [7] J. Haah, *Phys. Rev. A* **83**, 042330 (2011).
- [8] B. Yoshida, *Phys. Rev. B* **88**, 125122 (2013).
- [9] S. Vijay, J. Haah, and L. Fu, *Phys. Rev. B* **92**, 235136

Appendix A: Large K_z Degenerate Perturbation Theory

In this section, we will apply degenerate perturbation theory (DPT) (Appendix B) to the extended model H' (Eq. (25)) and produce a phase diagram (Fig. 11) in the limit when $K_z \gg \max(K_x, K_y)$. To reduce verbosity, throughout this section we will often refer to operators by their coefficient. For example, when we say that E_\square and t anticommute, we mean that an operator with coefficient E_\square anticommutes with an operator with coefficient t . We will perform DPT by splitting the Hamiltonian in Eq. (25) into $H' = H_0 + H_1$ where $|H_0| \gg |H_1|$ (where any operator norm can be chosen). K_z will always be included in H_0 , and K_x and K_y will always be in H_1 . Therefore, t can only be in H_0 if $t \gg \max(K_x, K_y)$; and t can only be in H_1 if $t \ll K_z$. Similarly, h can only be in H_0 if $h \gg \max(K_x, K_y)$; and h can only be in H_1 if $h \ll K_z$. These (overlapping) conditions partition (via the dotted gray lines) the phase diagram (Fig. 11) into four overlapping quadrants.

DPT will generate many different terms. But how do we determine the resulting phase? Instead of trying to answer this question direction, we will instead consider one target phase at a time (e.g. X-cube fracton order), and then attempt to calculate a sufficient condition for that phase (e.g. $\max(K_x, K_y) \ll t \ll K_z$). In our model, doing this is simplified because all terms in the Hamiltonian that we consider are products of Pauli operators, which we will refer to as Pauli strings. Furthermore, all of the phases that we're interested in are gapped and can be described by a stabilizer Hamiltonian. By stabilizer Hamiltonian, we will mean a Hamiltonian that is a sum of Pauli strings which all commute with each other. The ground state of the stabilizer Hamiltonian will also be the ground state of an extensive number of Pauli string terms in the stabilizer Hamiltonian; we will refer to these Pauli strings as stabilizers. Examples of stabilizer Hamiltonians are: $H = \sum_i X_i$ which stabilizes a paramagnet, $H = \sum_{\langle ij \rangle} Z_i Z_j$ which stabilizes a ferromagnet, or the toric code $H = \sum_{\square} \prod_{i \in \square} Z_i + \sum_{+} \prod_{i \in +} X_i$ which stabilizes Z_2 topological order. In certain limits, such as $\max(K_x, K_y) \ll t \ll K_z$ in Eq. (7), we will find that (multiple applications of) DPT produces a Hamiltonian that is a stabilizer Hamiltonian. If we obtain the right stabilizers, then we know that the limits considered are a sufficient condition for the target phase.

As a generic example, suppose we want to find sufficient conditions for a target phase with stabilizers: A_i , B_i , C_i , and D_i . If at least one of these operators appears in H , then we can apply DPT with at least one of them appearing in H_0 . Suppose only A_i appears in H with energy E_A . Then we must choose $H_0 = -\sum_i E_A A_i$. In order for DPT to converge, we will have to assume that E_A is much larger than all energies in H_1 . This will thus

be part of the sufficient condition for the target phase. If we assume this, and generate an effective Hamiltonian H_{eff} , then A_i will be a stabilizer (after more applications of DPT) of the ground state since H_{eff} resides in the degenerate ground state manifold of H_0 . Now suppose that $\sum_i E_B B_i$ is a term in H_{eff} , but neither C_i nor D_i appear. Then we will want to apply DPT to H_{eff} with $H'_0 = -\sum_i E_B B_i$ and $H'_1 = H_{\text{eff}} - H'_0$ to generate a new effective Hamiltonian H_{eff} in hope of eventually generating C_i and D_i . In order for DPT to converge, we will have to assume that E_B is larger than all other terms in H_{eff} . In particular, we will be most worried about terms which anticommute with B_i , since these terms will create excitations of B_i and will therefore try to prevent B_i from being a stabilizer. Suppose the new effective Hamiltonian H'_{eff} does include C_i and D_i with energies E_C and E_D , respectively. Then if E_C and E_D are sufficiently large, we can apply DPT once more with $H''_0 = -\sum_i (E_C C_i + E_D D_i)$, and we will be left with a stabilizer Hamiltonian of the desired phase. Note that terms like $\sum_{\langle ij \rangle} E_{CC} C_i C_j$ may also be generated. However, as long as $E_{CC} \ll E_C$, these terms don't affect the ground state, and so they will be ignored since $C_i C_j$ is not an independent stabilizer from C_i (since it's the product of C_i and C_j). Thus, a sufficient condition for the target phase would require that E_A , E_B , E_C , and E_D are sufficiently large.

In Fig. 11 we show the results from this approach. The sufficient conditions that we generate for each phase are not necessary conditions. Thus, we can not fill in the entire phase diagram (as seen in Fig. 8). However, Fig. 11 is drawn in a subspace of couplings (K_μ, t, h) where we can identify the phase at almost every point.

Below we list the energies (calculated in Appendix A 5) for the important terms generated by degenerate perturbation theory (DPT) that are required for drawing the phase diagram (Fig. 11).

$$\begin{aligned} E_\square &\sim \frac{K_x^2 K_y^2}{K_z \max(K_z, h)^2} \\ E_+ &\sim \frac{K_x^2 K_y^2}{\max(K_z, t)^4 / K_z} \end{aligned} \quad (\text{A1})$$

E_\square (introduced in Eq. (4)) corresponds to a toric code flux operator (Fig. 4) on an XY or XZ plane. E_+ (Eq. (4)) corresponds to a 2+1D toric code charge operator (Fig. 4) on an XY or XZ plane. The “ \sim ” in the expressions means that these expressions are only asymptotically correct; e.g. factors of two are ignored which allows simplifications such as $K_z + t \sim \max(K_z, t)$.

Energies for other terms generated by DPT will also be mentioned. These energies can be difficult to calculate in some cases due to the high order of DPT required to calculate them; but fortunately their values will not be important in this work. These energies are:

- E_{\square}^{YZ} (in Eq. (33) and (39)), corresponding to a toric code flux operator (Fig. 9) on a YZ plane
- E_{cube} (in Eq. (12)), corresponding to an X-cube fracton number operator (Fig. 6)
- E_* (in Eq. (33)), corresponding to a 3+1D toric code charge operator (Fig. 9)
- E_+^{YZ} (in Eq. (39)), corresponding to the same operator as E_* , but we instead view it as a YZ-plane toric code charge operator

We now apply DPT to H' (Eq. (25)) in various limits. $H_{h'}$ (Eq. (27)) will be considered as an example of a generic perturbation that can be added to break unphysical degeneracy which results in some cases; it's coefficient h' will always be assumed to be infinitesimally small. Then we will calculate E_{\square} and E_+ (Eq. (A1)) in Appendix A 5.

1. XY&XZ plane 2+1D Z_2 Topological Order

This phase occurs when K_z , E_{\square} , and E_+ are the stabilizers. Let us determine sufficient conditions for this. We'll need to do DPT in order to produce E_{\square} and E_+ . We'll do DPT with $H_0 = -K_z(\dots)$. To ensure that DPT converges, we'll need to assume $K_z \gg \max(K_x, K_y, t, h)$. E_{\square} and E_+ are the highest energy operators generated by DPT. But E_{\square} anticommutes with t , and can therefore only be a stabilizer if $E_{\square} \gg t$. And E_+ anticommutes with h , and can therefore only be a stabilizer if $E_+ \gg h$. Therefore, if

$$K_z \gg \max(K_x, K_y, t, h) \text{ and } E_{\square} \gg t \text{ and } E_+ \gg h \quad (\text{A2})$$

then another application of DPT with $H'_0 = -K_z(\dots) - E_{\square}(\dots) - E_+(\dots)$ will produce a stabilizer Hamiltonian with 2+1D Z_2 topological order along the original XY and XZ planes. The above conditions are already sufficient to ensure that DPT converges. This is the decoupled phase.

2. X-cube Fracton Topological Order

This phase occurs when K_z , t , E_{cube} , and E_+ are stabilizers. Let us determine sufficient conditions for this. We'll need to do DPT in order to produce E_{cube} and E_+ .

Let us first try DPT with $H_0 = -K_z(\dots) - t(\dots)$. To ensure that DPT converges, we'll need to assume $\min(K_z, t) \gg \max(K_x, K_y, h)$. E_+ is the highest energy operator generated by DPT. But E_+ anticommutes with h , and can therefore only be a stabilizer if $E_+ \gg h$. E_{cube} is the next highest energy operator generated by DPT that's independent from and commutes with the previous

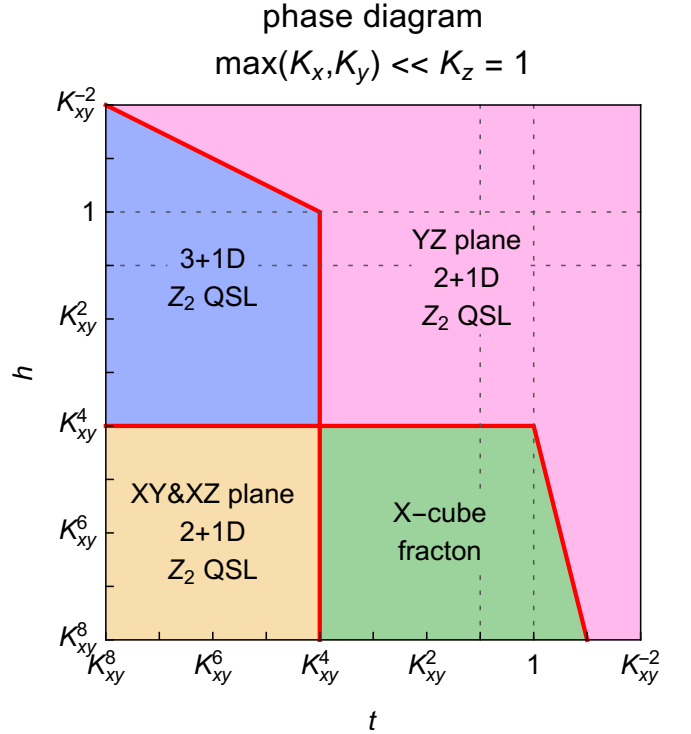


FIG. 11. Phase diagram of H' (Eq. (25)) in the limit $\max(K_x, K_y) \ll K_z = 1$ with $\max(K_x, K_y)/K_z$ infinitesimally small. Finite $\max(K_x, K_y)/K_z$ is shown in Fig. 3 and 8. Z_2 QSL is short for quantum spin liquid with Z_2 topological order. The 2+1D QSL phases are in the same phase as parallel layers of 2+1D toric code along certain orthogonal planes. The phase boundaries are calculated in Appendix A and given by Eq. (A2), (A3), (A4), and (A5). Degenerate perturbation theory does not determine the nature of the phase transitions, nor the possible existence of intermediate phases. However, duality arguments can be used to describe these transitions (Sec. III and Sec. IV C). The dotted gray lines separate overlapping regions where different choices of unperturbed Hamiltonian H_0 were used in degenerate perturbation theory in Appendix A. The diagram is a log-log plot where the axes have log base K_{xy}^{-1} where $K_{xy} = \sqrt{K_x K_y}$. (The axes are labeled by powers of K_{xy} , which is to be thought of as a very small number ϵ .) Note that the point set topology of the log-log coordinates in the $K_{xy} \ll K_z$ limit can be surprising. Specifically, for finite K_{xy}/K_z , intermediate phases are possible (see Appendix C), but in the $K_{xy} \ll K_z$ limit, these intermediate phases shrink into the red lines.

(candidate) stabilizers: K_z , t , and E_+ . (The product of two E_+ terms may be generated with a higher energy, but such terms will not affect the ground state since their energy is much smaller than E_+ .) E_{cube} can therefore be a stabilizer. In fact, if K_z , t , and E_+ are stabilizers, then E_{cube} will have to be a stabilizer if we require the ground state to be the ground state of a stabilizer Hamiltonian which is stable to arbitrary perturbations. There simply is no other Pauli string that commutes with K_z , t , and E_+ , and isn't a product of K_z , t , E_+ ,

and $E_{\mathbb{D}}$. Therefore, if $\min(K_z, t) \gg \max(K_x, K_y, h)$ and $E_+ \gg h$, then X-cube fracton topological order will be stabilized. That is, applying DPT again with $H'_0 = -K_z(\dots) - t(\dots) - E_{\mathbb{D}}(\dots) - E_+(\dots)$ will result in a stabilizer Hamiltonian with X-cube fracton order; the above assumptions are already sufficient to guarantee that DPT converges.

But what if it isn't the case that $t \gg \max(K_x, K_y, h)$? To cover this case, we'll also try DPT with $H_0 = -K_z(\dots)$. To ensure that DPT converges, we'll need to assume $K_z \gg \max(K_x, K_y, t, h)$. (This assumption will overlap with the $\min(K_z, t) \gg \max(K_x, K_y, h)$ assumption in the previous paragraph, but the results in this overlapping region are the same.) E_{\square} and E_+ are the highest energy operators generated by DPT. t anticommutes with E_{\square} , and can therefore only be a stabilizer if $t \gg E_{\square}$. We can do DPT again with $H'_0 = -t(\dots)$ and $H'_1 = -E_{\square}(\dots) - E_+(\dots) - h(\dots) + \dots$ where the last “...” denotes unimportant subleading terms. $t \gg E_{\square}$ (note $E_{\square} \sim E_+$) is already sufficient to ensure that DPT converges. E_+ anticommutes with h , and can therefore only be a stabilizer if $E_+ \gg h$. $E_{\mathbb{D}}$ is the highest energy operator generated by DPT that's independent from and commutes with the previous (candidate) stabilizers: K_z , t and E_+ . $E_{\mathbb{D}}$ can therefore be a stabilizer. Therefore, if $K_z \gg \max(K_x, K_y, t, h)$ and $t \gg E_{\square}$ and $E_+ \gg h$, then X-cube fracton topological order will be stabilized.

In summary, a sufficient condition for X-cube fracton topological order is

$$\begin{aligned} &[\min(K_z, t) \gg \max(K_x, K_y, h) \text{ and } E_+ \gg h] \text{ or} \\ &[K_z \gg \max(K_x, K_y, t, h) \text{ and } t \gg E_{\square} \text{ and } E_+ \gg h] \end{aligned} \quad (\text{A3})$$

3. 3+1D Z_2 Topological Order

This phase occurs when K_z , h , E_{\square} , E_{\square}^{YZ} , and E_* are the stabilizers. Let us determine sufficient conditions for this. We'll need to do DPT in order to produce E_{\square} , E_{\square}^{YZ} , and E_* .

Let us first try DPT with $H_0 = -K_z(\dots) - h(\dots)$. To ensure that DPT converges, we'll need to assume $\min(K_z, h) \gg \max(K_x, K_y, t)$. E_{\square} is the highest energy operator generated by DPT. But E_{\square} anticommutes with t , and can therefore only be a stabilizer if $E_{\square} \gg t$. $E_{\mathbb{D}}$ and E_* are the next highest energy operators generated by DPT that are independent from and commute with the previous (candidate) stabilizers: K_z , h , and E_{\square} . $E_{\mathbb{D}}$ and E_* can therefore be stabilizers since they commute. (If they anticommuted, then they couldn't both be stabilizers.) The current stabilizers (K_z , h , E_{\square} , E_* , and $E_{\mathbb{D}}$) describe a phase corresponding to 3+1D toric code, but without YZ-plane plaquette/flux operators. This phase is unstable to perturbations and has unphysical

degeneracy $\sim 2^{L^2}$ on a torus due to the L^2 missing E_{\square}^{YZ} operators on any single YZ plane. However, with generic perturbations (for which we choose $H_{h'}$ (Eq. (27)) as an example), we can do DPT again with $H'_0 = -E_{\square}(\dots) - E_*(\dots) - E_{\mathbb{D}}(\dots)$ and $H'_1 = H_{h'} + \dots$ where the last “...” denotes unimportant subleading terms. E_{\square}^{YZ} is the highest energy operator generated by DPT. E_{\square}^{YZ} can therefore be a stabilizer (which makes $E_{\mathbb{D}}$ a redundant stabilizer since it's the product of two E_{\square}^{YZ} operators, modulo K_z and h operators). Therefore, if $\min(K_z, h) \gg \max(K_x, K_y, t)$ and $E_{\square} \gg t$, then 3+1D Z_2 topological order will be stabilized.

But what if it isn't the case that $h \gg \max(K_x, K_y, t)$? To cover this case, we'll also try DPT with $H_0 = -K_z(\dots)$. To ensure that DPT converges, we'll need to assume $K_z \gg \max(K_x, K_y, t, h)$. (This assumption will overlap with the $\min(K_z, h) \gg \max(K_x, K_y, t)$ assumption in the previous paragraph, but the results in this overlapping region are the same.) E_{\square} and E_+ are the highest energy operators generated by DPT. But h anticommutes with E_+ , and can therefore only be a stabilizer if $h \gg E_+$. We can do DPT again with $H'_0 = -h(\dots)$ and $H'_1 = -E_{\square}(\dots) - E_+(\dots) - t(\dots) + \dots$. $h \gg E_+$ is already sufficient to ensure that DPT converges. E_{\square} anticommutes with t , and can therefore only be a stabilizer if $E_{\square} \gg t$. $E_{\mathbb{D}}$ and E_* are the highest energy operators generated by DPT that are independent from and commute with the previous (candidate) stabilizers: K_z , h and E_{\square} . $E_{\mathbb{D}}$ and E_* can therefore be stabilizers since they commute. We can do DPT again with $H''_0 = -h(\dots) - E_{\square}(\dots) - E_*(\dots) - E_{\mathbb{D}}(\dots)$ and $H''_1 = H_{h'} + \dots$. E_{\square}^{YZ} is the highest energy operator generated by DPT and can therefore be a stabilizer. Therefore, if $K_z \gg \max(K_x, K_y, t, h)$ and $h \gg E_+$ and $E_{\square} \gg t$, then 3+1D topological order will be stabilized.

In summary, a sufficient condition for 3+1D Z_2 topological order is

$$\begin{aligned} &[\min(K_z, h) \gg \max(K_x, K_y, t) \text{ and } E_{\square} \gg t] \text{ or} \\ &[K_z \gg \max(K_x, K_y, t, h) \text{ and } h \gg E_+ \text{ and } E_{\square} \gg t] \end{aligned} \quad (\text{A4})$$

when generic (but arbitrarily small) perturbations (such as H' (Eq. (25))) are included in the Hamiltonian H' (Eq. (25)).

4. YZ-plane 2+1D Z_2 topological order

This phase occurs when K_z , h , t , E_{\square}^{YZ} , and E_+^{YZ} are the stabilizers. Let us determine sufficient conditions for this. We'll need to do DPT in order to produce E_{\square}^{YZ} and E_+^{YZ} .

Let us first try DPT with $H_0 = -K_z(\dots) - t(\dots) + h(\dots)$. To ensure that DPT converges, we'll need to

assume $\min(K_z, t, h) \gg \max(K_x, K_y)$. E_+^{YZ} and E_{\square} are the highest energy operators generated by DPT. E_+^{YZ} and E_{\square} can therefore be stabilizers since they commute. The current stabilizers (K_z , h , E_+^{YZ} , and E_{\square}) describe a phase that is unstable to perturbations and has unphysical degeneracy $\sim 2^{L^2}$ on a torus due to the L^2 missing E_{\square}^{YZ} operators on any single YZ plane. However, with generic perturbations (for which we choose $H_{h'}$ (Eq. (27)) as an example), we can do DPT again with $H'_0 = -E_+^{YZ}(\dots) - E_{\square}(\dots)$ and $H'_1 = H_{h'} + \dots$ where the last “ \dots ” denotes unimportant subleading terms. E_{\square}^{YZ} is the highest energy operator generated by DPT and can therefore be a stabilizer. Therefore, if $\min(K_z, t, h) \gg \max(K_x, K_y)$, then the desired phase will be stabilized.

Let us now try DPT with $H_0 = -K_z(\dots) - t(\dots)$. To ensure that DPT converges, we'll need to assume $\min(K_z, t) \gg \max(K_x, K_y, h)$. E_+ is the highest energy operator generated by DPT. But h anticommutes with E_+ , and can therefore only be a stabilizer if $h \gg E_+$. E_+ and E_{\square} are the next highest energy operators generated by DPT that are independent from and commute with the previous (candidate) stabilizers: K_z , t , and h . E_+ and E_{\square} can therefore be stabilizers since they commute. We can do DPT again with $H'_0 = -h(\dots) - E_+(\dots) - E_{\square}(\dots)$ and $H'_1 = H_{h'} + \dots$. E_{\square}^{YZ} is the highest energy operator generated by DPT and can therefore be a stabilizer. Therefore, if $\min(K_z, t) \gg \max(K_x, K_y, h)$ and $h \gg E_+$, then the desired phase will be stabilized.

Let us now try DPT with $H_0 = -K_z(\dots) - h(\dots)$. To ensure that DPT converges, we'll need to assume $\min(K_z, h) \gg \max(K_x, K_y, t)$. E_{\square} is the highest energy operator generated by DPT. But t anticommutes with E_{\square} , and can therefore only be a stabilizer if $t \gg E_{\square}$. E_+^{YZ} and E_{\square} are the next highest energy operators generated by DPT that are independent from and commute with the previous (candidate) stabilizers: K_z , t , and h . E_+^{YZ} and E_{\square} can therefore be stabilizers since they commute. We can do DPT again with $H'_0 = -t(\dots) - E_+^{YZ}(\dots) - E_{\square}(\dots)$ and $H'_1 = H_{h'} + \dots$. E_{\square}^{YZ} is the highest energy operator generated by DPT and can therefore be a stabilizer. Therefore, if $\min(K_z, h) \gg \max(K_x, K_y, t)$ and $t \gg E_{\square}$, then the desired phase will be stabilized.

Let us now try DPT with $H_0 = -K_z(\dots)$. To ensure that DPT converges, we'll need to assume $K_z \gg \max(K_x, K_y, t, h)$. E_{\square} and E_+ are the highest energy operators generated by DPT. But t anticommutes with E_{\square} , and can therefore only be a stabilizer if $t \gg E_{\square}$. And h anticommutes with E_+ , and can therefore only be a stabilizer if $h \gg E_+$. We can do DPT again with $H'_0 = -t(\dots) - h(\dots)$ and $H'_1 = -E_{\square}(\dots) - E_+(\dots) + \dots$ where the last “ \dots ” denotes unimportant subleading terms. The previous assumptions are sufficient to ensure that DPT converges. E_{\square} and E_+^{YZ} are the highest energy operators generated by DPT that are independent from and commute with the previous (candidate) stabilizers:

K_z , t , and h . E_{\square} and E_+^{YZ} can therefore be stabilizers since they commute. We can do DPT again with $H''_0 = -t(\dots) - h(\dots) - E_+^{YZ}(\dots) - E_{\square}(\dots)$ and $H''_1 = H_{h'} + \dots$. E_{\square}^{YZ} is the highest energy operator generated by DPT and can therefore be a stabilizer. Therefore, if $K_z \gg \max(K_x, K_y, t, h)$ and $t \gg E_{\square}$ and $h \gg E_+$, then the desired phase will be stabilized.

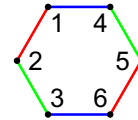
In summary, a sufficient condition for 2+1D Z_2 topological order on YZ planes is

$$\begin{aligned} & [\min(K_z, t, h) \gg \max(K_x, K_y)] \text{ or} \\ & [\min(K_z, t) \gg \max(K_x, K_y, h) \text{ and } h \gg E_+] \text{ or} \\ & [\min(K_z, h) \gg \max(K_x, K_y, t) \text{ and } t \gg E_{\square}] \text{ or} \\ & [K_z \gg \max(K_x, K_y, t, h) \text{ and } t \gg E_{\square} \text{ and } h \gg E_+] \end{aligned} \quad (\text{A5})$$

when generic (but arbitrarily small) perturbations (such as H' (Eq. (25))) are included in the Hamiltonian H' (Eq. (25)). Physically, when these perturbations are small, $E_{\square} \gg E_{\square}^{YZ}$ and this implies that in the excited states, flux excitations E_{\square}^{YZ} will want to be bound to a partner flux excitation on a neighboring layer. However, this does not change the resulting phase of the ground state.

5. E_{\square} and E_+ Calculation

In this section, we'll calculate E_{\square} and E_+ using degenerate perturbation theory (Appendix B). E_{\square} and E_+ appear in the effective Hamiltonian H^{eff} at fourth order, and the only term at this order that contributes is $\mathcal{P}(H_1 \mathcal{D})^3 H_1 \mathcal{P}$. We will focus on the E_{\square} or E_+ term that is generated for a single hexagon with indices labeled as shown below.



Thus, we only need to consider the terms of H_1 that act only on these six sites. And we can erase all Pauli operators from H_0 which aren't on one of these six sites. E_{\square} is centered on plaquettes (Fig. 4) and is calculated assuming $t \ll K_z$. Thus, we can take $t = 0$ when calculating E_{\square} , but we must consider the h term acting on sites 1 and 4, and 3 and 6. E_+ is centered on vertices (Fig. 4) and is calculated assuming $h \ll K_z$. Thus, we can take $h = 0$ when calculating E_+ , but we must consider the t term acting on sites 2 and 5. Therefore, we can calculate E_{\square} and E_+ at the same time by using the H_0 and H_1 below and taking either t or h equal to

zero.

$$\begin{aligned}
H_0 &= -(K_z + \frac{t}{2})(\sigma_2^z + \sigma_5^z) - K_z(\sigma_1^z \sigma_4^z + \sigma_3^z \sigma_6^z) \\
&\quad - \frac{h}{2}(\sigma_1^x \sigma_4^y + \sigma_1^y \sigma_4^x + \sigma_3^x \sigma_6^y + \sigma_3^y \sigma_6^x) \\
H_1 &= -K_x(\sigma_1^x \sigma_2^x + \sigma_5^x \sigma_6^x) - K_y(\sigma_2^y \sigma_3^y + \sigma_4^y \sigma_5^y)
\end{aligned}$$

The effective Hamiltonian is:

$$\begin{aligned}
H_4^{\text{eff}} &= \mathcal{P}H_1\mathcal{D}H_1\mathcal{D}H_1\mathcal{D}H_1\mathcal{P} \\
&= 8K_y\sigma_2^y\sigma_3^y\frac{-1}{4K_z+t+h}K_x\sigma_5^x\sigma_6^x\frac{-1}{4K_z+2t}K_y\sigma_4^y\sigma_5^y\frac{-1}{4K_z+t+h}K_x\sigma_1^x\sigma_2^x \\
&\quad + 8K_y\sigma_2^y\sigma_3^y\frac{-1}{4K_z+t+h}K_y\sigma_4^y\sigma_5^y\frac{-1}{8K_z+2t+2h}K_x\sigma_5^x\sigma_6^x\frac{-1}{4K_z+t+h}K_x\sigma_1^x\sigma_2^x \\
&= -E\sigma_1^x\sigma_2^z\sigma_3^y\sigma_4^y\sigma_5^z\sigma_6^x \\
&= -E\sigma_1^y\sigma_2^z\sigma_3^x\sigma_4^x\sigma_5^z\sigma_6^y
\end{aligned} \tag{A6}$$

$$E = \frac{4K_x^2K_y^2}{(4K_z+t+h)^2} \left(\frac{1}{2K_z+t} - \frac{1}{4K_z+t+h} \right) \tag{A7}$$

E_{\square} is given by E in Eq. (A7) with $t = 0$, which matches Eq. (A1) asymptotically. E_+ is given by E in Eq. (A7) with $h = 0$, which also matches Eq. (A1) asymptotically. Note that we used the fact that $\sigma_1^z\sigma_4^z = \sigma_3^z\sigma_6^z = 1$ in the low energy Hilbert space to get Eq. (A6) from the previous line, which matches the form of $[\sigma]_p^{\square xy}$ and $[\sigma]_l^{+xy}$ in Fig. 4.

Appendix B: Degenerate Perturbation Theory

In this section, we review the Schrieffer-Wolff formulation of degenerate perturbation theory [25, 26], which we use in the rest of the paper. We begin by splitting a Hamiltonian H into an unperturbed Hamiltonian H_0 and a perturbation λH_1 where $\lambda \ll 1$.

$$H = H_0 + \lambda H_1 \tag{B1}$$

We will focus on the case where H_0 has a degenerate ground state manifold with energy E_0 . The goal is to derive an effective Hamiltonian H^{eff} which describes the physics of the ground state manifold in the presence of the perturbation λH_1 .

We define an operator \mathcal{P} which projects onto the ground state manifold:

$$\mathcal{P}H_0 = H_0\mathcal{P} = E_0\mathcal{P} \tag{B2}$$

and define the effective Hamiltonian H^{eff} using a

canonical transformation on H

$$H^{\text{eff}} \equiv e^{+S} H e^{-S} \tag{B3}$$

$$\begin{aligned}
&= H + [S, H] + \frac{1}{2!}[S, [S, H]] + \frac{1}{3!}[S, [S, [S, H]]] + \dots \\
&= H_0 + \lambda \left([S_1, H_0] + \underbrace{H_1}_{X_1} \right) \\
&\quad + \lambda^2 \left([S_2, H_0] + \underbrace{[S_1, H_1] + \frac{1}{2!}[S_1, [S_1, H_0]]}_{X_2} \right) + \dots
\end{aligned}$$

$$S = \sum_{n=1}^{\infty} \lambda^n S_n \tag{B4}$$

$$X_n \equiv \frac{1}{n!} (\partial_{\lambda}^n H^{\text{eff}})_{\lambda \rightarrow 0} - [S_n, H_0]$$

The canonical transformation is generated by an anti-hermitian operator S . We also define X_n as shown above. With S defined as in Eq. (B4), in order for H^{eff} to capture the desired physics, it is sufficient to require that the effective Hamiltonian commutes with the ground state projection operator \mathcal{P} :

$$[\mathcal{P}, H^{\text{eff}}] = 0 \tag{B5}$$

This condition implies that the unitary rotation e^S has rotated H into H^{eff} with a block diagonal form such that the original ground state manifold is completely decoupled from the high energy Hilbert space. A solution

to Eq. (B5) exists in which S_n is defined iteratively in terms of S_1, S_2, \dots, S_{n-1} :

$$\begin{aligned} S_n &= \mathcal{P}X_n\mathcal{D} - \mathcal{D}X_n\mathcal{P} \\ \mathcal{D} &= -\frac{1 - \mathcal{P}}{H_0 - E_0} \end{aligned} \quad (\text{B6})$$

The disadvantage of this solution is that S is a nonlocal operator due to the presence of the nonlocal projection operator \mathcal{P} . Thus, when we calculate a series expansion for H^{eff} (Eq. (B9)), it will not be explicitly local. The locality of H^{eff} will only result from a precise cancellation due to minus signs.

We now define some compact notation:

$$\begin{aligned} \langle\langle \nu_1, \nu_2, \dots, \nu_n \rangle\rangle &\equiv \mathcal{D}^{(\nu_1)} H_1 \mathcal{D}^{(\nu_2)} H_1 \dots \mathcal{D}^{(\nu_n)} \\ \langle \nu_1, \nu_2, \dots, \nu_n \rangle &\equiv \langle\langle 0, \nu_1, \nu_2, \dots, \nu_n, 0 \rangle\rangle \\ &= \mathcal{P} H_1 \mathcal{D}^{(\nu_1)} H_1 \mathcal{D}^{(\nu_2)} H_1 \dots \mathcal{D}^{(\nu_n)} H_1 \mathcal{P} \\ \mathcal{D}^{(\nu)} &\equiv \begin{cases} \mathcal{P} & \nu = 0 \\ \mathcal{D}^\nu & \nu > 0 \end{cases} \end{aligned} \quad (\text{B7})$$

Using this notation and iterating Eq. (B6) on a computer gives the following expansion for the canonical transformation generator S and the effective Hamiltonian H^{eff} projected into the low energy Hilbert space:

$$\begin{aligned} S_1 &= \mathcal{P}H_1\mathcal{D} - \mathcal{D}H_1\mathcal{P} \\ &= \langle\langle 0, 1 \rangle\rangle - \langle\langle 1, 0 \rangle\rangle \\ S_2 &= \mathcal{P}H_1\mathcal{D}H_1\mathcal{D} - \mathcal{D}H_1\mathcal{D}H_1\mathcal{P} - \mathcal{P}H_1\mathcal{P}H_1\mathcal{D}^2 + \mathcal{D}^2H_1\mathcal{P}H_1\mathcal{P} \\ &= \langle\langle 0, 1, 1 \rangle\rangle - \langle\langle 1, 1, 0 \rangle\rangle - \langle\langle 0, 0, 2 \rangle\rangle + \langle\langle 2, 0, 0 \rangle\rangle \\ S_3 &= \langle\langle 0, 1, 1, 1 \rangle\rangle - \langle\langle 1, 1, 1, 0 \rangle\rangle \\ &\quad - \langle\langle 0, 0, 1, 2 \rangle\rangle - \langle\langle 0, 0, 2, 1 \rangle\rangle - \langle\langle 0, 1, 0, 2 \rangle\rangle - \frac{1}{3}\langle\langle 0, 2, 0, 1 \rangle\rangle + \frac{1}{3}\langle\langle 1, 0, 2, 0 \rangle\rangle + \langle\langle 1, 2, 0, 0 \rangle\rangle + \langle\langle 2, 0, 1, 0 \rangle\rangle + \langle\langle 2, 1, 0, 0 \rangle\rangle \\ &\quad + \langle\langle 0, 0, 0, 3 \rangle\rangle - \langle\langle 3, 0, 0, 0 \rangle\rangle \\ S_4 &= \langle\langle 0, 1, 1, 1, 1 \rangle\rangle - \langle\langle 1, 1, 1, 1, 0 \rangle\rangle \\ &\quad - \langle\langle 0, 0, 1, 1, 2 \rangle\rangle - \langle\langle 0, 0, 1, 2, 1 \rangle\rangle - \langle\langle 0, 0, 2, 1, 1 \rangle\rangle - \langle\langle 0, 1, 0, 1, 2 \rangle\rangle - \langle\langle 0, 1, 0, 2, 1 \rangle\rangle - \langle\langle 0, 1, 1, 0, 2 \rangle\rangle - \frac{1}{3}\langle\langle 0, 1, 2, 0, 1 \rangle\rangle \\ &\quad - \frac{1}{3}\langle\langle 0, 2, 0, 1, 1 \rangle\rangle - \frac{1}{3}\langle\langle 0, 2, 1, 0, 1 \rangle\rangle + \frac{1}{3}\langle\langle 1, 0, 1, 2, 0 \rangle\rangle + \frac{1}{3}\langle\langle 1, 0, 2, 1, 0 \rangle\rangle + \frac{1}{3}\langle\langle 1, 1, 0, 2, 0 \rangle\rangle + \langle\langle 1, 1, 2, 0, 0 \rangle\rangle \\ &\quad + \langle\langle 1, 2, 0, 1, 0 \rangle\rangle + \langle\langle 1, 2, 1, 0, 0 \rangle\rangle + \langle\langle 2, 0, 1, 1, 0 \rangle\rangle + \langle\langle 2, 1, 0, 1, 0 \rangle\rangle + \langle\langle 2, 1, 1, 0, 0 \rangle\rangle \\ &\quad + \langle\langle 0, 0, 0, 2, 2 \rangle\rangle + \langle\langle 0, 0, 2, 0, 2 \rangle\rangle + \frac{1}{3}\langle\langle 0, 2, 0, 0, 2 \rangle\rangle - \frac{1}{3}\langle\langle 2, 0, 0, 2, 0 \rangle\rangle - \langle\langle 2, 0, 2, 0, 0 \rangle\rangle - \langle\langle 2, 2, 0, 0, 0 \rangle\rangle \\ &\quad + \langle\langle 0, 0, 0, 1, 3 \rangle\rangle + \langle\langle 0, 0, 0, 3, 1 \rangle\rangle + \langle\langle 0, 0, 1, 0, 3 \rangle\rangle + \frac{1}{3}\langle\langle 0, 0, 3, 0, 1 \rangle\rangle + \langle\langle 0, 1, 0, 0, 3 \rangle\rangle + \frac{1}{3}\langle\langle 0, 3, 0, 0, 1 \rangle\rangle \\ &\quad - \frac{1}{3}\langle\langle 1, 0, 0, 3, 0 \rangle\rangle - \frac{1}{3}\langle\langle 1, 0, 3, 0, 0 \rangle\rangle - \langle\langle 1, 3, 0, 0, 0 \rangle\rangle - \langle\langle 3, 0, 0, 1, 0 \rangle\rangle - \langle\langle 3, 0, 1, 0, 0 \rangle\rangle - \langle\langle 3, 1, 0, 0, 0 \rangle\rangle \\ &\quad - \langle\langle 0, 0, 0, 0, 4 \rangle\rangle + \langle\langle 4, 0, 0, 0, 0 \rangle\rangle \end{aligned} \quad (\text{B8})$$

$$\mathcal{P}H^{\text{eff}}\mathcal{P} = \sum_{n=0}^{\infty} \lambda^n H_n^{\text{eff}} \quad (\text{B9})$$

$$H_0^{\text{eff}} = E_0$$

$$H_1^{\text{eff}} = \mathcal{P}H_1\mathcal{P} = \langle \rangle$$

$$H_2^{\text{eff}} = \mathcal{P}H_1\mathcal{D}H_1\mathcal{P} = \langle 1 \rangle$$

$$\begin{aligned} H_3^{\text{eff}} &= \mathcal{P}H_1\mathcal{D}H_1\mathcal{D}H_1\mathcal{P} - \frac{1}{2}\mathcal{P}H_1\mathcal{P}H_1\mathcal{D}^2H_1\mathcal{P} - \frac{1}{2}\mathcal{P}H_1\mathcal{D}^2H_1\mathcal{P}H_1\mathcal{P} \\ &= \langle 1, 1 \rangle - \frac{1}{2}\langle 0, 2 \rangle - \frac{1}{2}\langle 2, 0 \rangle \end{aligned}$$

$$H_4^{\text{eff}} = \langle 1, 1, 1 \rangle - \frac{1}{2}\langle 0, 1, 2 \rangle - \frac{1}{2}\langle 0, 2, 1 \rangle - \frac{1}{2}\langle 1, 0, 2 \rangle - \frac{1}{2}\langle 1, 2, 0 \rangle - \frac{1}{2}\langle 2, 0, 1 \rangle - \frac{1}{2}\langle 2, 1, 0 \rangle + \frac{1}{2}\langle 0, 0, 3 \rangle + \frac{1}{2}\langle 3, 0, 0 \rangle$$

$$\begin{aligned} H_5^{\text{eff}} &= \langle 1, 1, 1, 1 \rangle - \frac{1}{2}\langle 0, 1, 1, 2 \rangle - \frac{1}{2}\langle 0, 1, 2, 1 \rangle - \frac{1}{2}\langle 0, 2, 1, 1 \rangle - \frac{1}{2}\langle 1, 0, 1, 2 \rangle - \frac{1}{2}\langle 1, 0, 2, 1 \rangle - \frac{1}{2}\langle 1, 1, 0, 2 \rangle - \frac{1}{2}\langle 1, 1, 2, 0 \rangle \\ &\quad - \frac{1}{2}\langle 1, 2, 0, 1 \rangle - \frac{1}{2}\langle 1, 2, 1, 0 \rangle - \frac{1}{2}\langle 2, 0, 1, 1 \rangle - \frac{1}{2}\langle 2, 1, 0, 1 \rangle - \frac{1}{2}\langle 2, 1, 1, 0 \rangle \\ &\quad + \frac{1}{2}\langle 0, 0, 2, 2 \rangle + \frac{3}{8}\langle 0, 2, 0, 2 \rangle + \frac{1}{4}\langle 2, 0, 0, 2 \rangle + \frac{3}{8}\langle 2, 0, 2, 0 \rangle + \frac{1}{2}\langle 2, 2, 0, 0 \rangle \\ &\quad + \frac{1}{2}\langle 0, 0, 1, 3 \rangle + \frac{1}{2}\langle 0, 0, 3, 1 \rangle + \frac{1}{2}\langle 0, 1, 0, 3 \rangle + \frac{1}{2}\langle 1, 0, 0, 3 \rangle + \frac{1}{2}\langle 1, 3, 0, 0 \rangle + \frac{1}{2}\langle 3, 0, 0, 1 \rangle + \frac{1}{2}\langle 3, 0, 1, 0 \rangle + \frac{1}{2}\langle 3, 1, 0, 0 \rangle \\ &\quad - \frac{1}{2}\langle 0, 0, 0, 4 \rangle - \frac{1}{2}\langle 4, 0, 0, 0 \rangle \end{aligned}$$

$$\begin{aligned} H_6^{\text{eff}} &= \langle 1, 1, 1, 1, 1 \rangle - \frac{1}{2}\langle 0, 1, 1, 1, 2 \rangle - \frac{1}{2}\langle 0, 1, 1, 2, 1 \rangle - \frac{1}{2}\langle 0, 1, 2, 1, 1 \rangle - \frac{1}{2}\langle 0, 2, 1, 1, 1 \rangle - \frac{1}{2}\langle 1, 0, 1, 1, 2 \rangle - \frac{1}{2}\langle 1, 0, 1, 2, 1 \rangle \\ &\quad - \frac{1}{2}\langle 1, 0, 2, 1, 1 \rangle - \frac{1}{2}\langle 1, 1, 0, 1, 2 \rangle - \frac{1}{2}\langle 1, 1, 0, 2, 1 \rangle - \frac{1}{2}\langle 1, 1, 1, 0, 2 \rangle - \frac{1}{2}\langle 1, 1, 1, 2, 0 \rangle - \frac{1}{2}\langle 1, 1, 2, 0, 1 \rangle \\ &\quad - \frac{1}{2}\langle 1, 1, 2, 1, 0 \rangle - \frac{1}{2}\langle 1, 2, 0, 1, 1 \rangle - \frac{1}{2}\langle 1, 2, 1, 0, 1 \rangle - \frac{1}{2}\langle 1, 2, 1, 1, 0 \rangle - \frac{1}{2}\langle 2, 0, 1, 1, 1 \rangle - \frac{1}{2}\langle 2, 1, 0, 1, 1 \rangle \\ &\quad - \frac{1}{2}\langle 2, 1, 1, 0, 1 \rangle - \frac{1}{2}\langle 2, 1, 1, 1, 0 \rangle \\ &\quad + \frac{1}{2}\langle 0, 0, 1, 2, 2 \rangle + \frac{1}{2}\langle 0, 0, 2, 1, 2 \rangle + \frac{1}{2}\langle 0, 0, 2, 2, 1 \rangle + \frac{1}{2}\langle 0, 1, 0, 2, 2 \rangle + \frac{3}{8}\langle 0, 1, 2, 0, 2 \rangle + \frac{3}{8}\langle 0, 2, 0, 1, 2 \rangle + \frac{3}{8}\langle 0, 2, 0, 2, 1 \rangle \\ &\quad + \frac{3}{8}\langle 0, 2, 1, 0, 2 \rangle + \frac{1}{2}\langle 1, 0, 0, 2, 2 \rangle + \frac{3}{8}\langle 1, 0, 2, 0, 2 \rangle + \frac{1}{4}\langle 1, 2, 0, 0, 2 \rangle + \frac{3}{8}\langle 1, 2, 0, 2, 0 \rangle + \frac{1}{2}\langle 1, 2, 2, 0, 0 \rangle \\ &\quad + \frac{1}{4}\langle 2, 0, 0, 1, 2 \rangle + \frac{1}{4}\langle 2, 0, 0, 2, 1 \rangle + \frac{1}{4}\langle 2, 0, 1, 0, 2 \rangle + \frac{3}{8}\langle 2, 0, 1, 2, 0 \rangle + \frac{3}{8}\langle 2, 0, 2, 0, 1 \rangle + \frac{3}{8}\langle 2, 0, 2, 1, 0 \rangle \\ &\quad + \frac{1}{4}\langle 2, 1, 0, 0, 2 \rangle + \frac{3}{8}\langle 2, 1, 0, 2, 0 \rangle + \frac{1}{2}\langle 2, 1, 2, 0, 0 \rangle + \frac{1}{2}\langle 2, 2, 0, 0, 1 \rangle + \frac{1}{2}\langle 2, 2, 0, 1, 0 \rangle + \frac{1}{2}\langle 2, 2, 1, 0, 0 \rangle \\ &\quad + \frac{1}{2}\langle 0, 0, 1, 1, 3 \rangle + \frac{1}{2}\langle 0, 0, 1, 3, 1 \rangle + \frac{1}{2}\langle 0, 0, 3, 1, 1 \rangle + \frac{1}{2}\langle 0, 1, 0, 1, 3 \rangle + \frac{1}{2}\langle 0, 1, 0, 3, 1 \rangle + \frac{1}{2}\langle 0, 1, 1, 0, 3 \rangle + \frac{1}{2}\langle 1, 0, 0, 1, 3 \rangle \\ &\quad + \frac{1}{2}\langle 1, 0, 0, 3, 1 \rangle + \frac{1}{2}\langle 1, 0, 1, 0, 3 \rangle + \frac{1}{2}\langle 1, 1, 0, 0, 3 \rangle + \frac{1}{2}\langle 1, 1, 3, 0, 0 \rangle + \frac{1}{2}\langle 1, 3, 0, 0, 1 \rangle + \frac{1}{2}\langle 1, 3, 0, 1, 0 \rangle \\ &\quad + \frac{1}{2}\langle 1, 3, 1, 0, 0 \rangle + \frac{1}{2}\langle 3, 0, 0, 1, 1 \rangle + \frac{1}{2}\langle 3, 0, 1, 0, 1 \rangle + \frac{1}{2}\langle 3, 0, 1, 1, 0 \rangle + \frac{1}{2}\langle 3, 1, 0, 0, 1 \rangle + \frac{1}{2}\langle 3, 1, 0, 1, 0 \rangle \\ &\quad + \frac{1}{2}\langle 3, 1, 1, 0, 0 \rangle \\ &\quad - \frac{1}{2}\langle 0, 0, 0, 2, 3 \rangle - \frac{1}{2}\langle 0, 0, 0, 3, 2 \rangle - \frac{1}{2}\langle 0, 0, 2, 0, 3 \rangle - \frac{3}{8}\langle 0, 0, 3, 0, 2 \rangle - \frac{3}{8}\langle 0, 2, 0, 0, 3 \rangle + \frac{1}{8}\langle 0, 2, 0, 3, 0 \rangle - \frac{1}{8}\langle 0, 3, 0, 0, 2 \rangle \\ &\quad + \frac{1}{8}\langle 0, 3, 0, 2, 0 \rangle - \frac{1}{4}\langle 2, 0, 0, 0, 3 \rangle - \frac{1}{8}\langle 2, 0, 0, 3, 0 \rangle - \frac{3}{8}\langle 2, 0, 3, 0, 0 \rangle - \frac{1}{2}\langle 2, 3, 0, 0, 0 \rangle - \frac{1}{4}\langle 3, 0, 0, 0, 2 \rangle \\ &\quad - \frac{3}{8}\langle 3, 0, 0, 2, 0 \rangle - \frac{1}{2}\langle 3, 0, 2, 0, 0 \rangle - \frac{1}{2}\langle 3, 2, 0, 0, 0 \rangle \\ &\quad - \frac{1}{2}\langle 0, 0, 0, 1, 4 \rangle - \frac{1}{2}\langle 0, 0, 0, 4, 1 \rangle - \frac{1}{2}\langle 0, 0, 1, 0, 4 \rangle - \frac{1}{2}\langle 0, 1, 0, 0, 4 \rangle - \frac{1}{2}\langle 1, 0, 0, 0, 4 \rangle - \frac{1}{2}\langle 1, 4, 0, 0, 0 \rangle - \frac{1}{2}\langle 4, 0, 0, 0, 1 \rangle \\ &\quad - \frac{1}{2}\langle 4, 0, 0, 1, 0 \rangle - \frac{1}{2}\langle 4, 0, 1, 0, 0 \rangle - \frac{1}{2}\langle 4, 1, 0, 0, 0 \rangle \\ &\quad + \frac{1}{2}\langle 0, 0, 0, 0, 5 \rangle + \frac{1}{2}\langle 5, 0, 0, 0, 0 \rangle \end{aligned}$$

Appendix C: Monte Carlo of Dual Ising Theories

In this appendix, we use classical Monte Carlo to provide evidence that the weakly coupled stacks of transverse-field Ising models that describe the dual phase transitions in Fig. 1 are likely to be first order. There are two cases to consider, 1) a weakly coupled 1D stack of 2+1D Ising models (as in Sec. III A), and 2) a weakly coupled 2D grid of 1+1D Ising models (as in Sec. III B). A classical Ising model in 3D and 2D will be used to simulate the 2+1D and 1+1D (respectively) zero temperature transverse field Ising model layers.

I and J will be used to denote the 3D or 2D lattice coordinate, while L will denote the layer (of the 1D stack or 2D grid). Thus, we will be interested in the following classical layered Ising-like model (with inverse temperature $\beta = 1$):

$$\begin{aligned}
 H_{\text{Ising}} &= -J \sum_L \sum_{\langle IJ \rangle} \sigma_{LI} \sigma_{LJ} & (C1) \\
 &- K \sum_{\langle LL' \rangle} \sum_{\langle IJ \rangle} \sigma_{LI} \sigma_{LJ} \sigma_{L'I} \sigma_{L'J} \\
 &= - \sum_L \sum_{\langle IJ \rangle} \underbrace{\left(J + K \sum_{\langle LL' \rangle} \sigma_{L'I} \sigma_{L'J} \right)}_{J_{LIJ}^{\text{eff}}} \sigma_{LI} \sigma_{LJ} & (C2)
 \end{aligned}$$

\sum_L sums over the layers and $\sum_{\langle IJ \rangle}$ sums over nearest-neighbor sites. The J term is a nearest-neighbor ferromagnetic Ising coupling that only couples spins on the same layer, where J is roughly related by $J \sim E_{\square}/t$ in Eq. (19) or $J \sim h/E_+$ in Eq. (24). The K term is a 4-spin term which couples together neighbor-neighbor spins or neighboring layers, and roughly corresponds to a product of two $[\tilde{\sigma}]_p^{\square_{xy}}$ or two $[\tilde{\tau}]_p^{\square_{xz}}$ operators in Sec. III A, or $J \sim E_{\square}^{YZ}/E_+$ in Eq. (24). It is useful to rewrite H_{Ising} as in Eq. (C2) to reveal that the K term results in a new effective J term (J_{LIJ}^{eff}) which is site and layer dependent. $\sum_{\langle LL' \rangle}$ sums over all layers L' which neighbor the layer L .

If $K = 0$, then the layers are decoupled and every layer independently undergoes an order to disorder transition. If K is small and positive, then we can see from the form of J_{LIJ}^{eff} that when a layer transitions into its ordered state, the average J_{LIJ}^{eff} for neighboring layers will increase. Thus, positive K causes the effective J to increase rapidly at the disorder to order transitions when J is increased. It is reasonable that this could lead to a first order transition.

If K is small and negative, then when a layer transitions into its ordered state, the average J_{LIJ}^{eff} for neighboring layers will decrease. This makes it difficult for the system to order all at once. What happens instead for intermediate J is that only half the layers order such

that ordered layers neighbor disordered layers, and visa versa. Thus, K makes the average J_{LIJ}^{eff} smaller only for the disordered layers. In Sec. C1, we will briefly discuss what these phases correspond to in the original model.

From the form of Eq. (C2) we see that each layer is an Ising model with a site-dependent coupling J_{LIJ}^{eff} . Therefore, we can apply the global Wolff update algorithm [27] to this model one layer at a time. Thus, it is easy to generalize Wolff update code to efficiently study this model even when the correlation length along the layers is large. However, since the update is only applied to one layer at a time, the update is effectively local across the layers. Thus, if the correlation length across the layers is large, the simulation will be inefficient. This can occur when the layer coupling K is large; however, since we are interested in weak layer coupling K , this isn't a major issue.

After applying this algorithm [28], we find that all of the transitions appear to be first order. The simulation results are summarized in Fig. 12. The figure shows that at every phase transition, ξ_c/L tends to decrease as the system size L increases, where ξ_c is the connected correlation length between two spins on the same layer. [29] (At a continuous phase transition, ξ_c/L would instead asymptote to a constant.) We also find other signs of discontinuous phase transitions, such as magnetization histograms with two bumps, which indicates the presence of metastable states and hysteresis effects which occur in discontinuous transitions. However, we can not rule out the possibility that smaller K could instead result in a continuous phase transition. Indeed, our smaller K looks second order at the currently simulated lattice sizes; however, we expect that larger lattices would then likely show signs of discontinuous phase transitions.

1. Intermediate Phases

From Fig. 12 we see that when the layer coupling K is negative, there is an intermediate phase where the squared layer magnetization $\langle S_L^2 \rangle \sim 1/2$, where $S_L \equiv \frac{1}{N_I} \sum_I \sigma_{LI}$ is the average magnetization on a given layer L . As previously mentioned, this phase spontaneously breaks translation symmetry and is characterized by a checkerboard pattern where half of the layers order, while the other half remain disordered. This can be described by the following order parameter

$$\begin{aligned}
 R &\equiv \frac{1}{N'} \sum_L \sum_{\langle IJ \rangle} (-1)^L \sigma_{LI} \sigma_{LJ} & (C3) \\
 N' &\equiv \sum_L \sum_{\langle IJ \rangle} 1
 \end{aligned}$$

In Fig. 13 we show that this order parameter R is nonzero only in the intermediate phase.

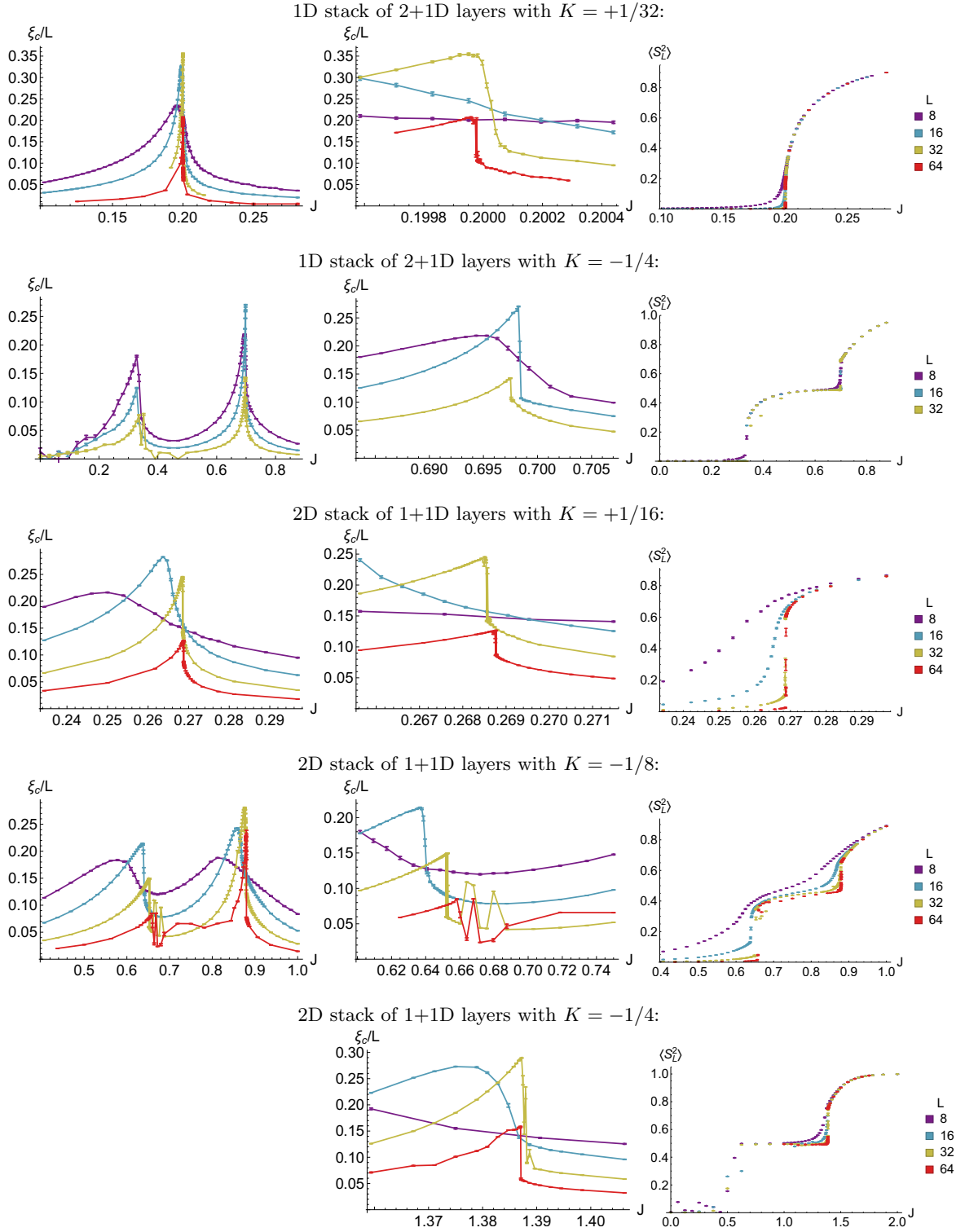


FIG. 12. The first column of plots shows ξ_c/L vs the ferromagnetic Ising coupling J , where ξ_c is the connected correlation length between two spins on the same layer. The second column is a closeup of a phase transition. The third column is the squared layer magnetization $\langle S_L^2 \rangle$ vs J , where $S_L \equiv \frac{1}{N_I} \sum_I \sigma_{LI}$ is the average magnetization on a given layer. The system size is $L \times L \times L \times L$. Each row corresponds to a different dimension for each layer, or different sign of K . All phase transitions appear to be first order since at each transition, ξ_c/L tends to decrease as the system length L increases. An exception is the second transition for the 2D stack of 1+1D layers with $K = -1/8$ (4th row and 1st column of plots, near $J \sim 0.88$). However, when K is increased to $K = -1/4$, the transition looks first order. (When $K = -1/4$, we cannot accurately measure the correlation length below $J \sim 1.2$ due to large autocorrelation times in this region.) We expect that larger system sizes would show that the $K = -1/8$ transition is also second order. Some of the data is a little messy (e.g. not smooth vs J) due to a loss of ergodicity (due to large autocorrelation times) near the first order transitions, which is a well known shortcoming of the Wolff MC update algorithm near a first order phase transition. (The one standard deviation statistical error bars do not account for this error.) All data points used at least 2^{12} MC sweeps. The second row used 2^{16} sweeps.

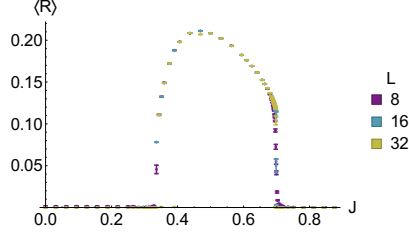
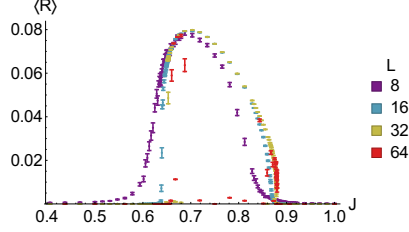
1D stack of 2+1D layers with $K = -1/4$:2D stack of 1+1D layers with $K = -1/8$:

FIG. 13. We show that the order parameter R (Eq. (C3)) describes the intermediate phase.

These intermediate phases of the layered Ising models are dual phases of phases in the original fracton model. We can determine which phase results in the original model by adding a term to the dual Ising model which explicitly breaks the symmetry that is spontaneously broken in the intermediate phase, and then apply the appropriate duality mapping (Eq. (18), 23 or 45) in reverse. To explicitly break the symmetry, we add the

following term to H_{Ising} (Eq. (C1)):

$$H_{\text{inter}}^{\text{dual}} = -F \sum_L \sum_{\langle IJ \rangle}^{\text{odd}} \sigma_{LI} \sigma_{LJ} \quad (\text{C4})$$

where F is a large constant and \sum_L^{odd} only sums over every other layer (in a checkerboard pattern). If we are interested in the 1+1D duality (Sec. III A), then we apply Eq. (18) and find that $H_{\text{inter}}^{\text{dual}}$ is dual to

$$H_{\text{inter}}^{1+1\text{D}} = -F \sum_{\text{x-axis } \ell}^{y+z \text{ odd}} \hat{\rho}_\ell^z \quad (\text{C5})$$

where $\sum_{\text{x-axis } \ell}^{y+z \text{ odd}}$ only sums over x-axis links ℓ with odd $y + z$. To describe the intermediate phase between X-cube order and YZ-plane 2+1D Z_2 QSL (intermediate #4 in Tab. I), we can add $H_{\text{inter}}^{1+1\text{D}}$ to $\hat{H}_{\text{X-cube}}$ (Eq. (21)) and apply degenerate perturbation theory (DPT) using $H_{\text{inter}}^{1+1\text{D}}$ as the unperturbed Hamiltonian. This will generate a Hamiltonian which describes the intermediate phase. This process can be repeated to generate Hamiltonians for the possible intermediate phases for all four phase transitions shown in Fig. 1. We do not write down these Hamiltonians here, nor have we analyzed what kind of topological order is present in these models. However, we have calculated their ground state degeneracies, which we show in Tab. I. This was done via a computer program [30] on finite lattices; we then extrapolated to arbitrary lattice sizes.

phase	XY&XZ plane 2+1D Z_2 QSL	intermediate #1	3+1D Z_2 QSL	intermediate #2	YZ-plane 2+1D Z_2 QSL
degeneracy	$2^{2L_y+2L_z}$	2×2^6	2^3	2×2^{L_x}	2^{2L_x}
phase		intermediate #3	X-cube	intermediate #4	
degeneracy		$2 \times 2^{L_x+2L_y+2L_z-3}$	$2^{2L_x+2L_y+2L_z-3}$	$2 \times 2^{2L_x+3}$	

TABLE I. Ground state degeneracies for the four phases in Fig. 1, along with the four possible intermediate phases that can occur. For example, intermediate #3 can occur between the 2+1D Z_2 QSL and X-cube phases. The degeneracies of all of the intermediate phases take the form $2 \times \dots$. The first factor of two in the degeneracies is not topological, and occurs due to the spontaneous translation symmetry breaking of the intermediate phase. The rest of the degeneracy is topological.